SUPPORTING INFORMATION

for

High-efficiency enzymatic biodegradation of polypropylene-based melt-blown fabric debris

Xiu Huang,[a,b] Li Huang,[a] Qian Wang,[a] Qiurong He[a], Zunzhen Zhang[a], Qian Liu,[b,c*] Guibin Jiang[b,c]

[a] West China School of Public Health and West China Fourth Hospital, Sichuan University, Sichuan 610041, China

[b] State Key Laboratory of Environmental Chemistry and Ecotoxicology, Research Center for Eco-Environmental Sciences, Chinese Academy of Sciences, Beijing 100085, China

[c] College of Resources and Environment, University of Chinese Academy of Sciences, Beijing 100190, China

[*]Correspondence: qianliu@rcees.ac.cn

Contents

Supporting tables

Table S1. Fitting results and parameters of the kinetic curve for the degradation of MBFD by trypsin and GST.[a]

MBFD	Condition	Curve parameter		
		a	*b*	R^2
Trypsin	37 °C, dark	82.4 ± 6.0	0.17 ± 0.05	0.905
WW-trypsin	37 °C, dark	371.7 ± 47.0	0.02 ± 0.01	0.980
GST	37 °C, dark	168.5 ± 69.3	0.05 ± 0.03	0.980
WW-GST	37 °C, dark	86.1 ± 0.2	0.43 ± 0.01	0.926

[a] First order kinetics model: $y=a(1-\exp(-bx))$, where b represents the rate constant. Multiplying this by the maximum concentration yields the maximum degradation rate.

Table S2. Feature MS peaks and peak ratios in **Fig. 3** used to deduce different degradation pathways in **Fig. 4**.

Oxidation	$C_2H_5O/C_3H_7O_2$, $C_2H_5O/[C_3H_6O_2+Na-2H]$, $C_5H_{10}O/C_6H_{12}O_2$, $C_6H_{11}O/[C_7H_{14}O_2+Na-2H]$, $C_8H_{17}O/C_9H_{18}O_2$, $[CH_2+Na-2H]/C_2H_5O$, $[CH_3+Na-H]/C_2H_5O$, $[C_2H_2+K-2H]/C_3H_6O$, $[C_2H_2+K-2H]/C_3H_7O$, $[C_2H_2+K-2H]/[C_3H_6O+Na-2H]$, $[C_5H_{10}+Na-H]/C_6H_{11}O$, $[C_7H_{15}+Na-H]/C_8H_{17}O$, $C_8H_{16}/C_9H_{18}O$, $C_2H_2/C_3H_7O_2$, $C_2H_2/[C_3H_6O_2+Na-2H]$, $[C_2H_2+K-2H]/C_3H_7O_2$, $[C_2H_2+K-2H]/[C_3H_6O_2+Na-2H]$, $C_5H_{11}/C_6H_{12}O_2$, $C_6H_{12}/[C_7H_{14}O_2+Na-2H]$, $C_8H_{16}/C_9H_{18}O_2$, $C_2H_5O/C_3H_7O_3$, $C_5H_{10}O/[C_6H_{12}O_3+Na-2H]$, C_2H_5O/C_2H_2, $C_2H_5O/[C_2H_2+K-2H]$, C_3H_6O/C_3H_5, C_3H_6O/C_3H_6, C_3H_7O/C_3H_6, C_3H_7O/C_3H_7, $[C_3H_6O+Na-2H]/C_3H_5$, $[C_3H_6O+Na-2H]/C_3H_6$, $C_5H_{10}O/C_5H_{11}$, $C_6H_{11}O/C_6H_{12}$, $C_8H_{17}O/C_8H_{16}$, $C_3H_7O_2/C_3H_7$, $[C_3H_6O_2+Na-2H]/C_3H_5$, $C_3H_7O_2/C_3H_6$, $[C_3H_6O_2+Na-2H]/C_3H_6$, $C_6H_{12}O_2/C_6H_{12}$, $C_3H_7O_2/[C_3H_6O+Na-2H]$, $[C_3H_6O_2+Na-2H]/[C_3H_6O+Na-2H]$, $C_3H_7O_2/C_3H_6O$, $C_3H_7O_2/C_3H_7O$, $[C_3H_6O_2+Na-2H]/C_3H_6O$, $C_6H_{12}O_2/C_6H_{11}O$, $C_9H_{18}O_2/C_9H_{18}O$, $C_3H_7O_3/C_3H_6O$, $C_3H_7O_3/[C_3H_6O+Na-2H]$, $C_3H_7O_3/C_3H_7O$, $[C_2H_4O_3+Na-2H]/C_2H_5O$, $C_5H_{11}O_3/C_5H_{10}O$, $[C_6H_{12}O_3+Na-2H]/C_6H_{11}O$, $C_3H_7O_3/C_3H_7O_2$, $[C_6H_{12}O_3+Na-2H]/C_6H_{12}O_2$
N-involved oxidation	$C_3H_7O_2/C_4H_8NO_2$, $C_2H_3NO/C_3H_7NO_2$, $[C_3H_6O_2+Na-2H]/C_4H_8NO_2$, $C_6H_{12}O_2/C_7H_{16}N_2O_2$, C_2H_3NO/C_2H_5O, $C_5H_{11}NO/C_5H_{10}O$, $C_5H_{10}NO/C_5H_{10}O$, $C_3H_7N_2O_2/[C_3H_6O_2+Na-2H]$, $C_3H_7N_2O_2/C_3H_7O_2$, $C_3H_7NO_2/[C_3H_6O_2+Na-2H]$, $C_3H_7NO_2/C_3H_7O_2$, $C_7H_{16}N_2O_2/[C_7H_{14}O_2+Na-2H]$, $[C_2H_4NO_2+K-2H]/C_2H_3NO$, $C_3H_7N_2O_2/C_3H_7NO_2$
Carbon cluster	$[C_{25}]$, $[C_{24}]$, $[C_{23}]$, $[C_{22}]$, $[C_{17}]$, $[C_{16}]$, $[C_{14}]$, $[C_{13}]$, $[C_{12}]$, $[C_{11}]$, $[C_9]$, $[C_8]$, $[C_7]$, $[C_6]$, $[C_5]$, $[C_4]$, $[C_3]$, $[C_2]$

Table S3. Typical peaks of GC-MS chromatogram and their corresponding mass spectra.

Serial number	Retention time (min)	*m/z*	Molecular formula	Compound
1	9.846	286	$C_{16}H_{30}O_4$	Oxalic acid, 2-ethylhexyl hexyl ester
2	14.352	256	$C_{16}H_{32}O_2$	n-Hexadecanoic acid
3	16.467	340	$C_{23}H_{32}O_2$	Phenol,2,2'-methylenebis[6-(1,1-dimethylethyl)-4-methyl
4	15.310	284	$C_{18}H_{36}O_2$	Octadecanoic acid
5	14.989	424	$C_{29}H_{60}O$	Eicosyl nonyl ether
6	11.865	206	$C_{14}H_{22}O$	2,4-Di-tert-butylphenol
7	9.897	134	$C_9H_{10}O$	Benzaldehyde
8	18.172	337	$C_{22}H_{43}NO$	13-Docosenamide
9	9.682	170	$C_{12}H_{26}$	Dodecane
10	12.011	212	$C_{15}H_{32}$	Pentadecane
11	15.929	338	$C_{24}H_{50}$	Tetracosane
12	10.155	184	$C_{13}H_{28}$	Tridecane
13	11.213	268	$C_{19}H_{40}$	Nonadecane
14	11.729	226	$C_{16}H_{34}$	Hexadecane
15	12.405	296	$C_{21}H_{44}$	Heneicosane
16	15.492	282	$C_{20}H_{42}$	Eicosane
17	10.888	198	$C_{14}H_{30}$	2,3-Dimethyldodecane
18	13.558	394	$C_{28}H_{58}$	Octacosane
19	11.371	240	$C_{17}H_{36}$	Heptadecane

Supporting figures

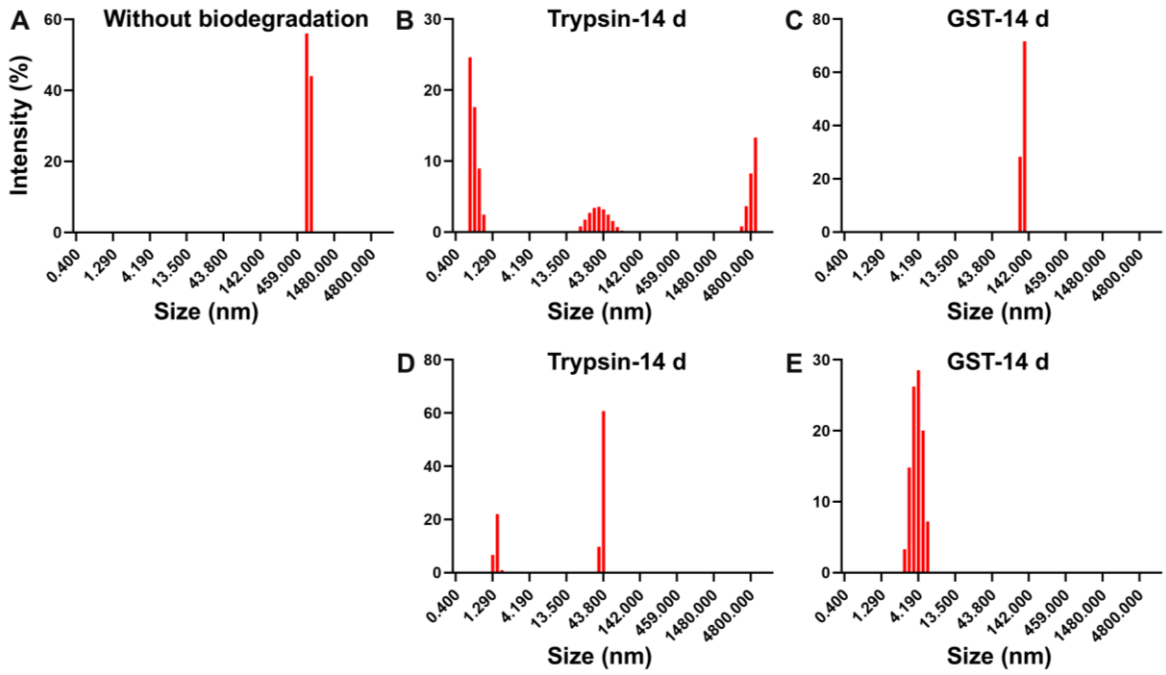

Figure S1. The particle size of MBFD in the water obtained by DLS under (A-C) dark conditions and (D-E) light conditions. DLS spectra of MBFD A) without biodegradation, (B, D) degraded by trypsin after incubating 14 days, and (C, E) degraded by GST after incubating 14 days. This result confirms the decreasing trend in particle size variation, transitioning from the micrometer to the nanometer scale. This aligns with the data presented on particle frequency.

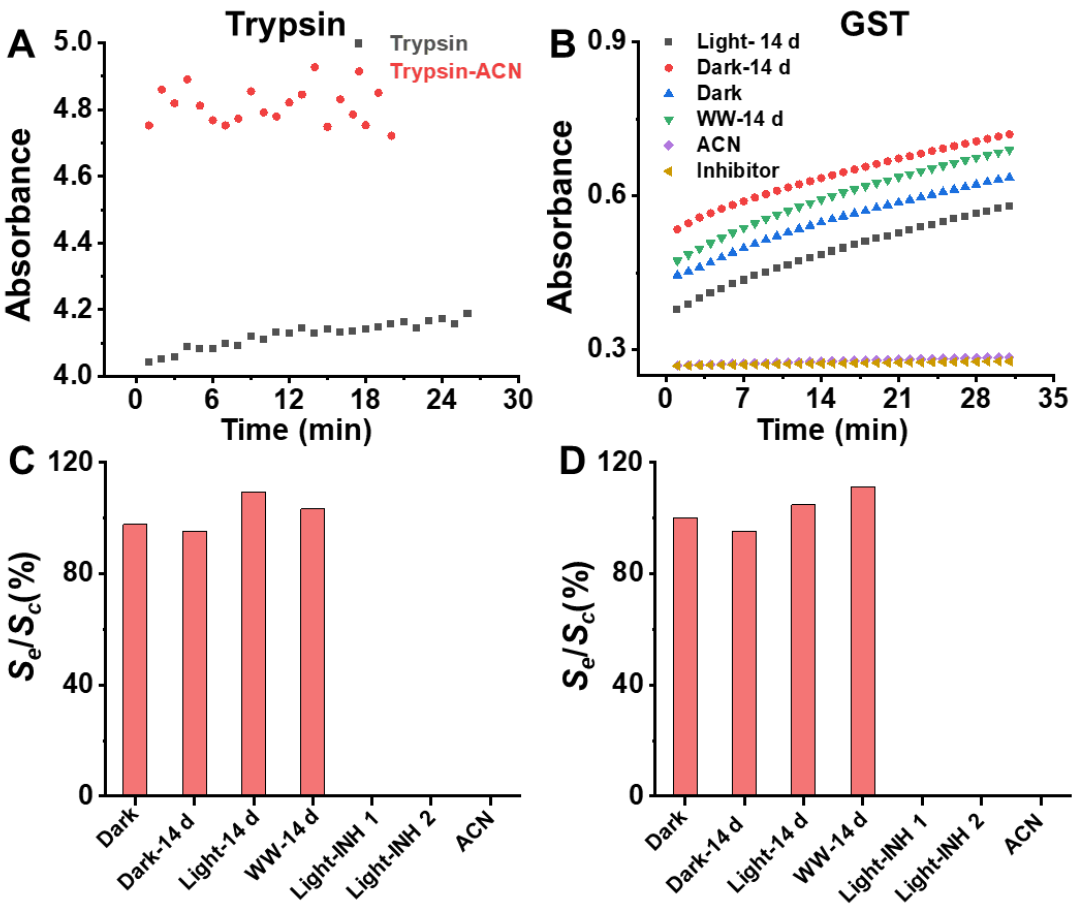

Figure S2. Comparison of the enzyme activity of trypsin and GST in the degradation of MBFD under different conditions. It can be seen that the activity of GST was inhibited in the presence of inhibitors or ACN.

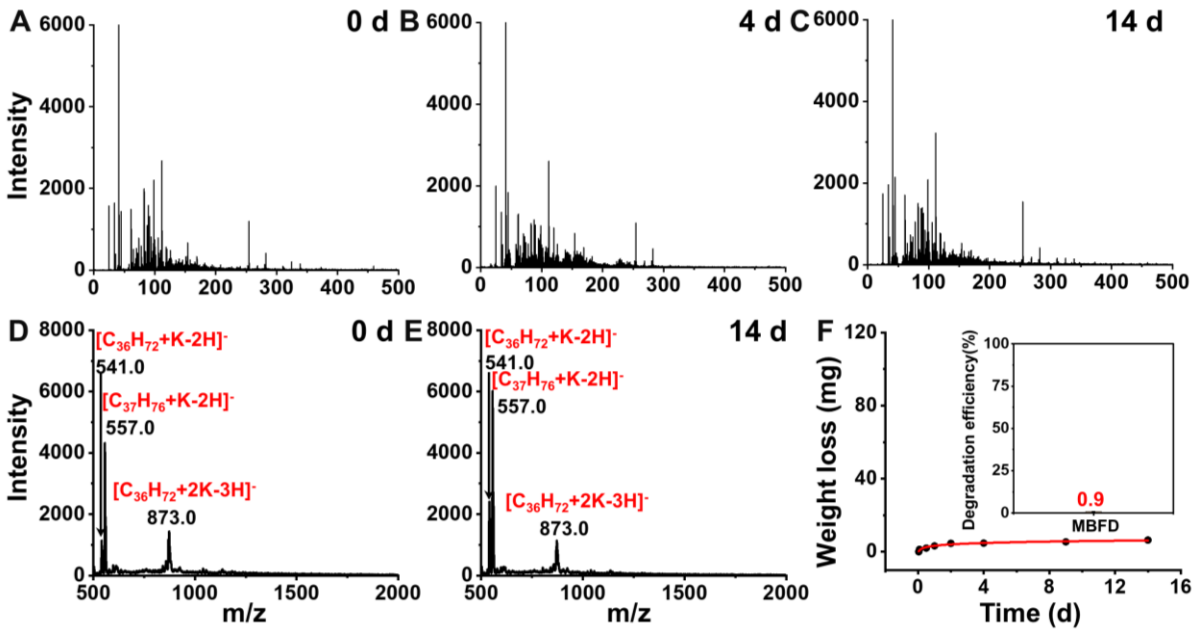

Figure S3. Monitoring the enzymatic depolymerization of MBFD in the presence of CYP450. MS spectra of MBFD in (A-C) low-mass region and (D-E) high-mass region degraded by CYP450 under dark conditions (37 °C) with an incubation time of 0-14 days. F) Degradation kinetics and degradation efficiency of MBFD. Degradation efficiency refers to the percentage of degraded polymer mass in the initial polymer mass, and it was calculated by the following equation: Degradation efficiency = 1 - (residual polymer mass/initial polymer mass).

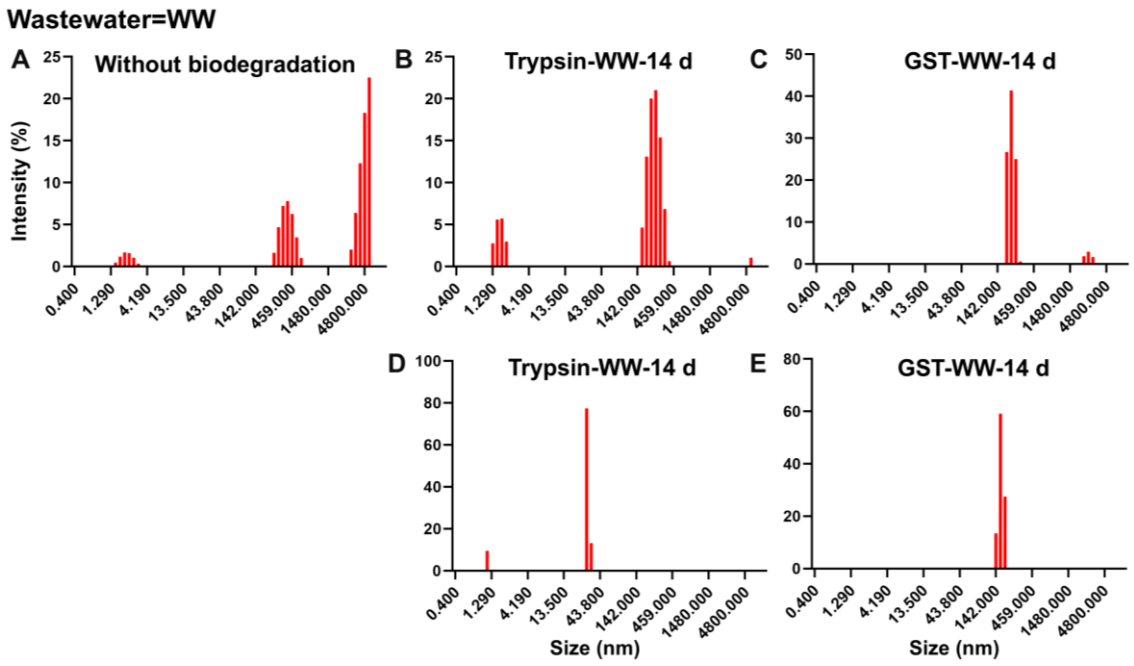

Figure S4. The particle size of MBFD in the wastewater (WW) obtained by DLS under (A-C) dark conditions and (D-E) light conditions. DLS spectra of MBFD A) without biodegradation, (B, D) degraded by trypsin after incubating 14 days, and (C, E) degraded by GST after incubating 14 days.

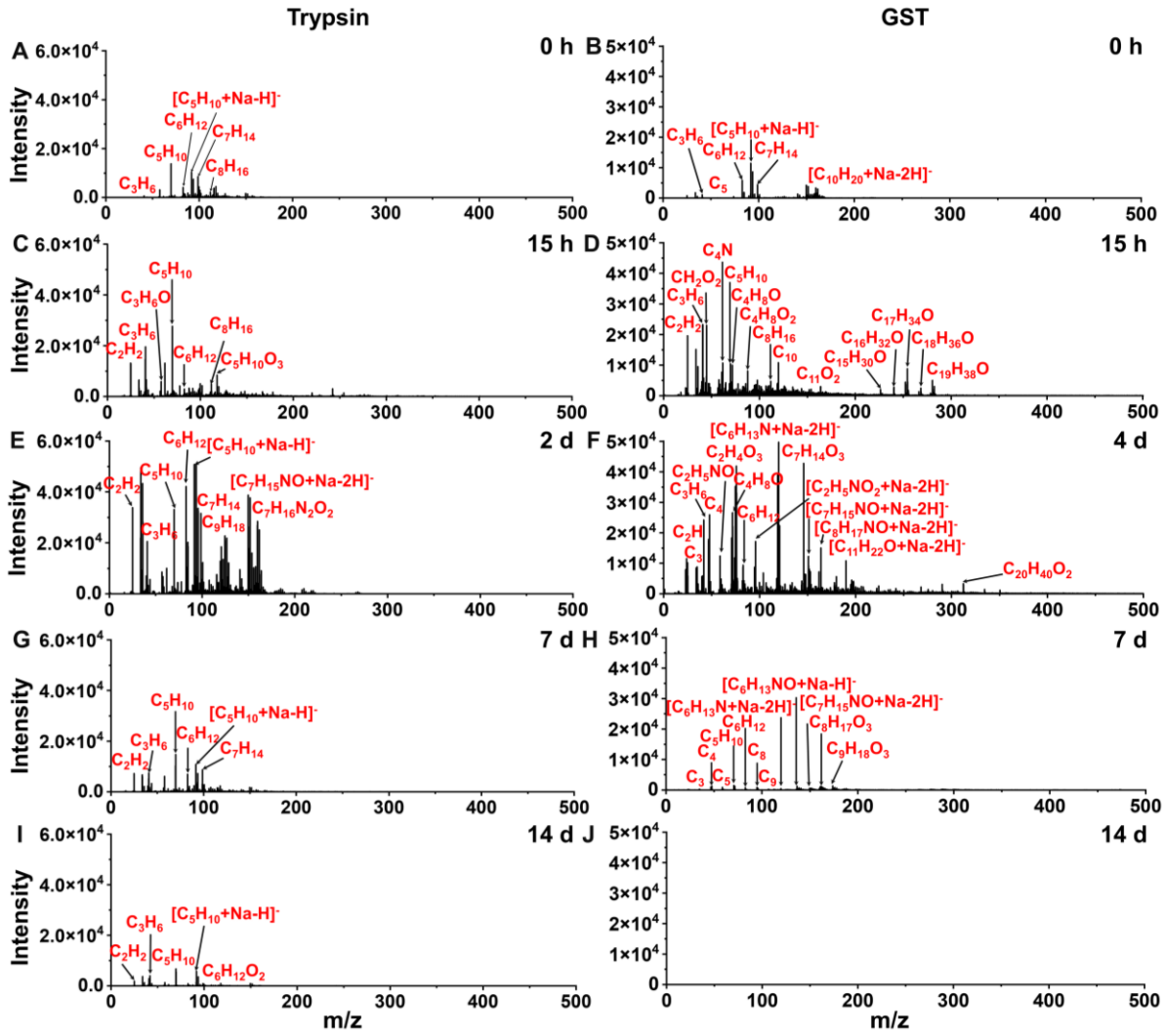

Figure S5. MS fingerprinting of MBFD degraded by trypsin and GST under different conditions. MS spectra of MBFD incubated for up to 14 days with trypsin (A, C, E, G, and I) and GST (B, D, F, H, and J).

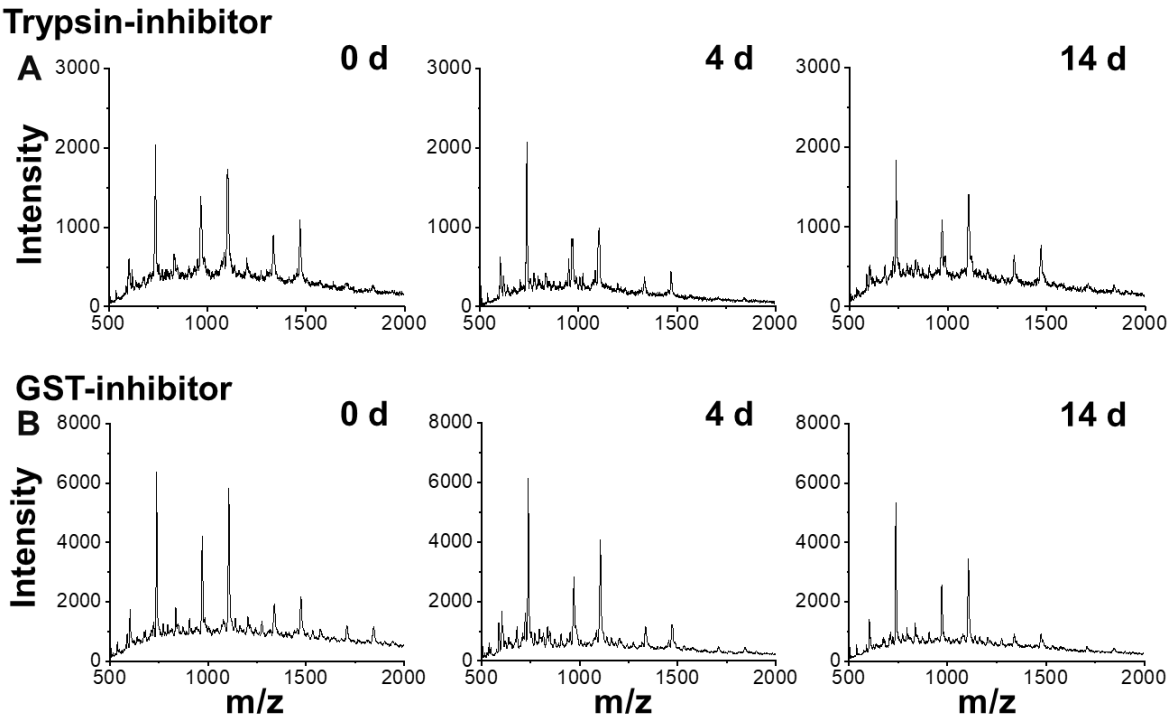

Figure S6. MS spectra of MBFD in high-mass region degraded by A) trypsin and B) GST in the presence of inhibitor over time (0 d, 4 d, and 14 d) under dark conditions (37 °C).

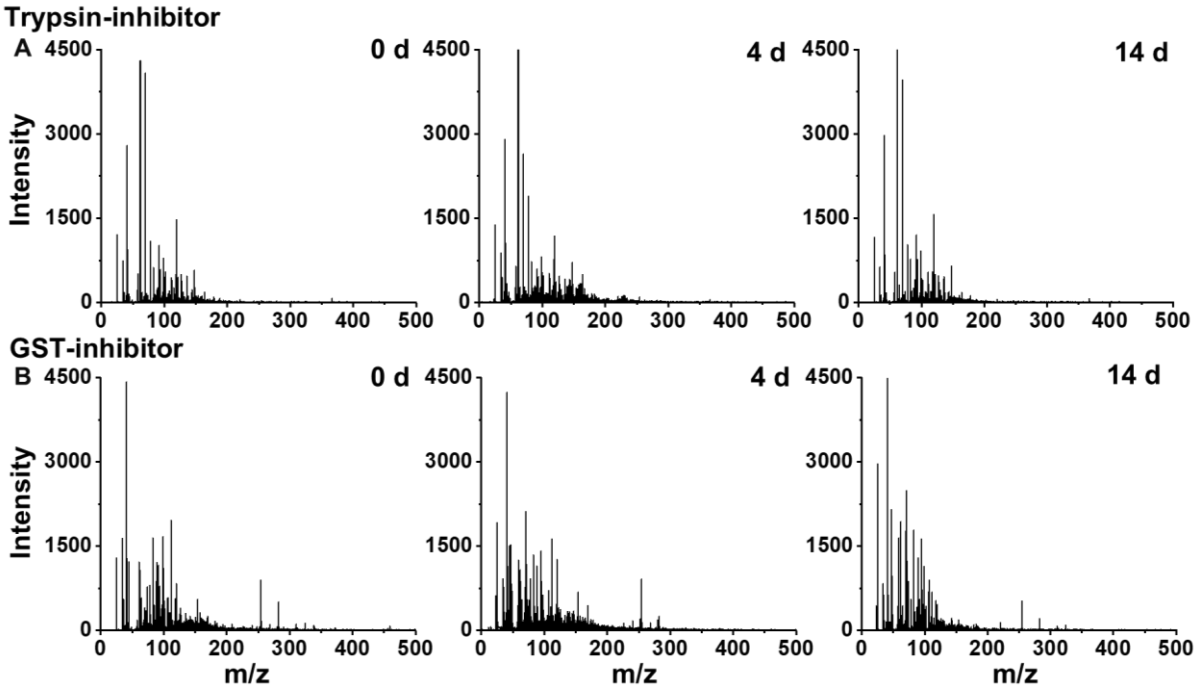

Figure S7. MS spectra of MBFD in low-mass region degraded by A) trypsin and B) GST in the presence of inhibitor over time (0 d, 4 d, and 14 d) under dark conditions (37 °C).

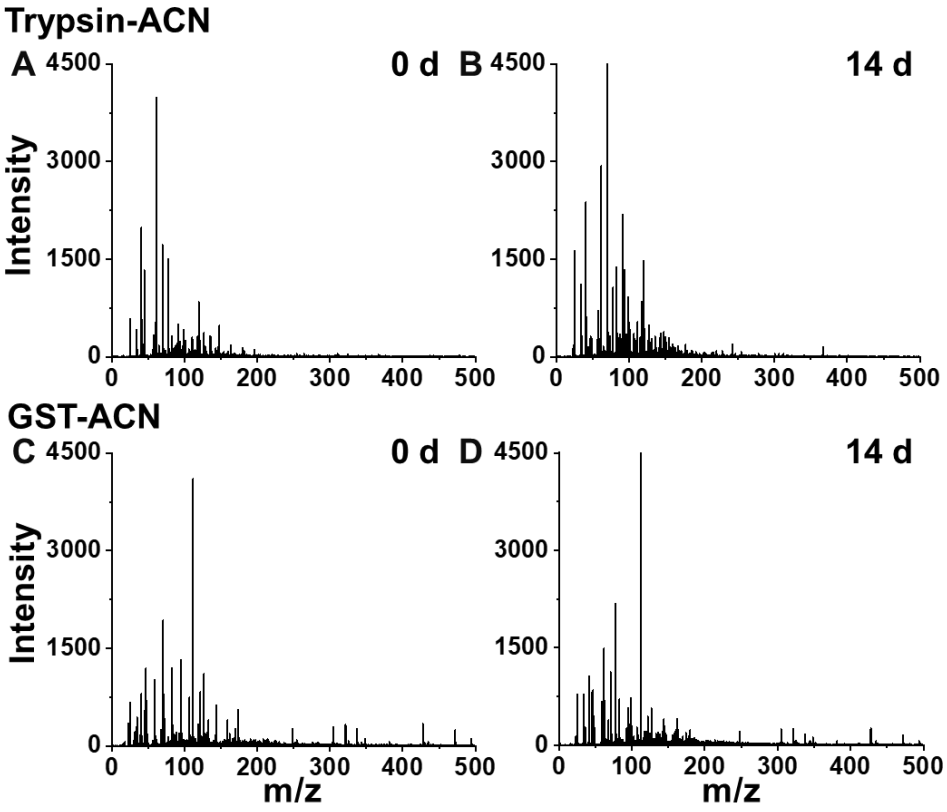

Figure S8. MS spectra of MBFD in low-mass region degraded by (A-B) trypsin and (C-D) GST incubated in ACN over time (0 d and 14 d) under dark conditions (37 °C).

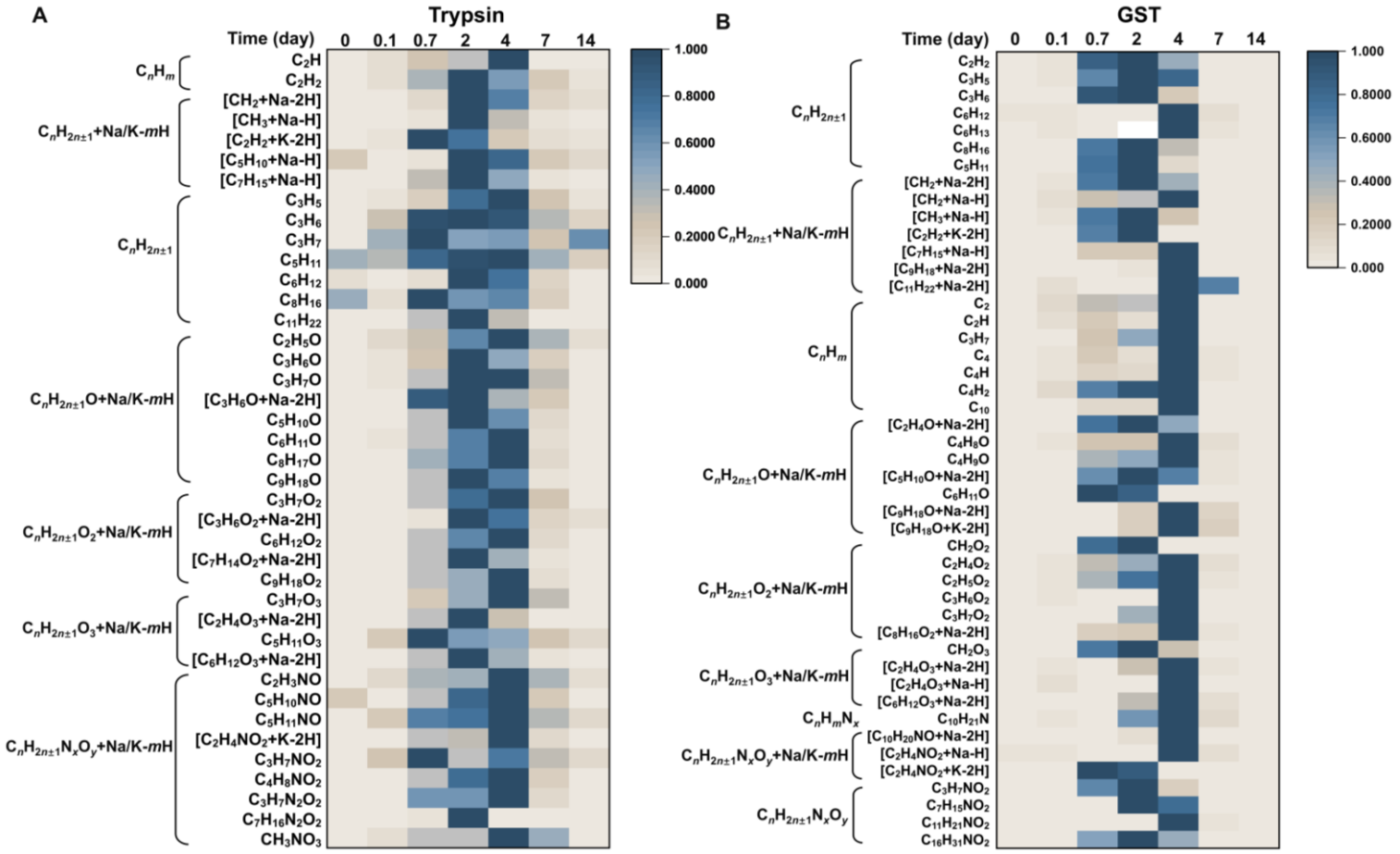

Figure S9. LDI-TOF MS fingerprinting of the degradation process of MBFD by trypsin and GST. Heat map of typical fingerprint peaks of MBFD by A) trypsin and B) GST during the degradation at physiological temperature for 14 days.

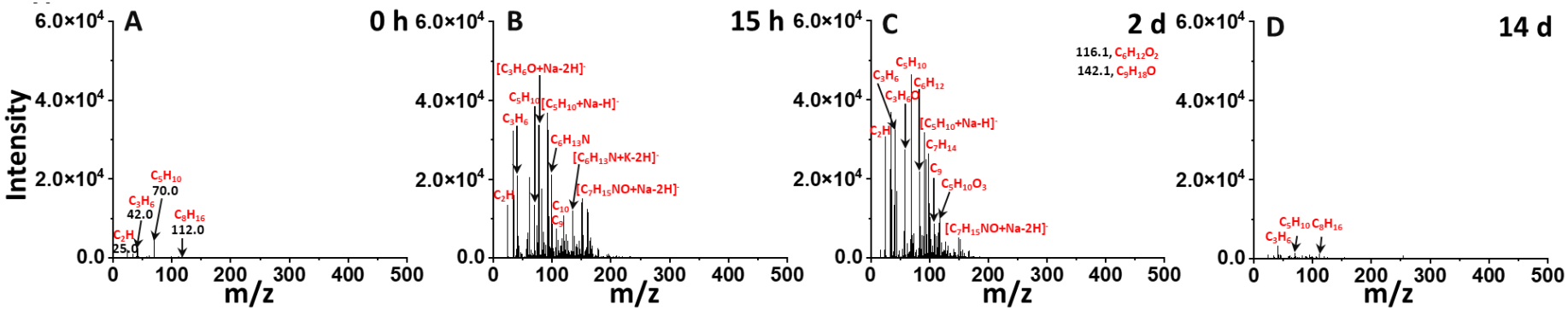

Figure S10. MS fingerprinting of MBFD in the wastewater degraded by trypsin. (A-D) Comparison of MS performance of MBFD degraded by trypsin over time (0-14 d). A) 0 h, B) 15 h, C) 2 d, D) 14 d.

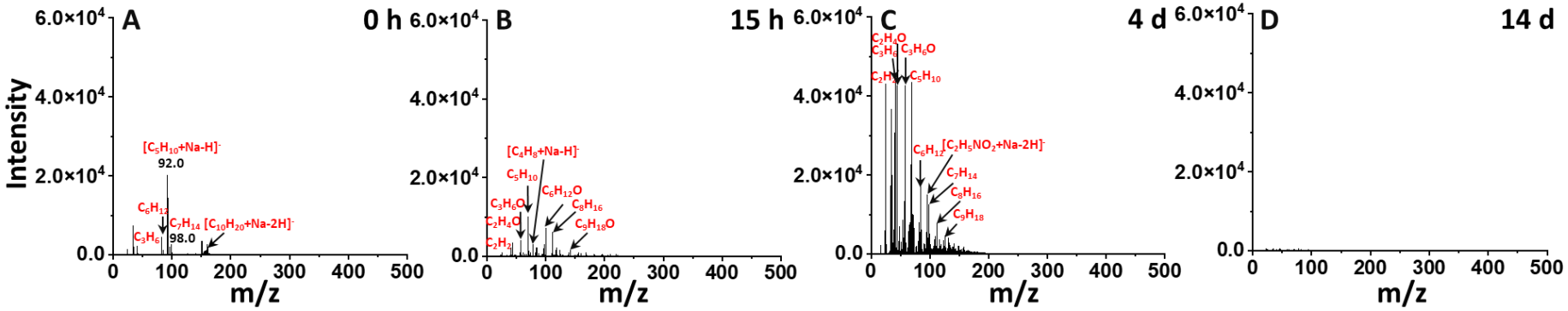

Figure S11. MS fingerprinting of MBFD in the wastewater degraded by GST. (A-D) Comparison of MS performance of MBFD degraded by GST over time (0-14 d). A) 0 h, B) 15 h, C) 4 d, D) 14 d.

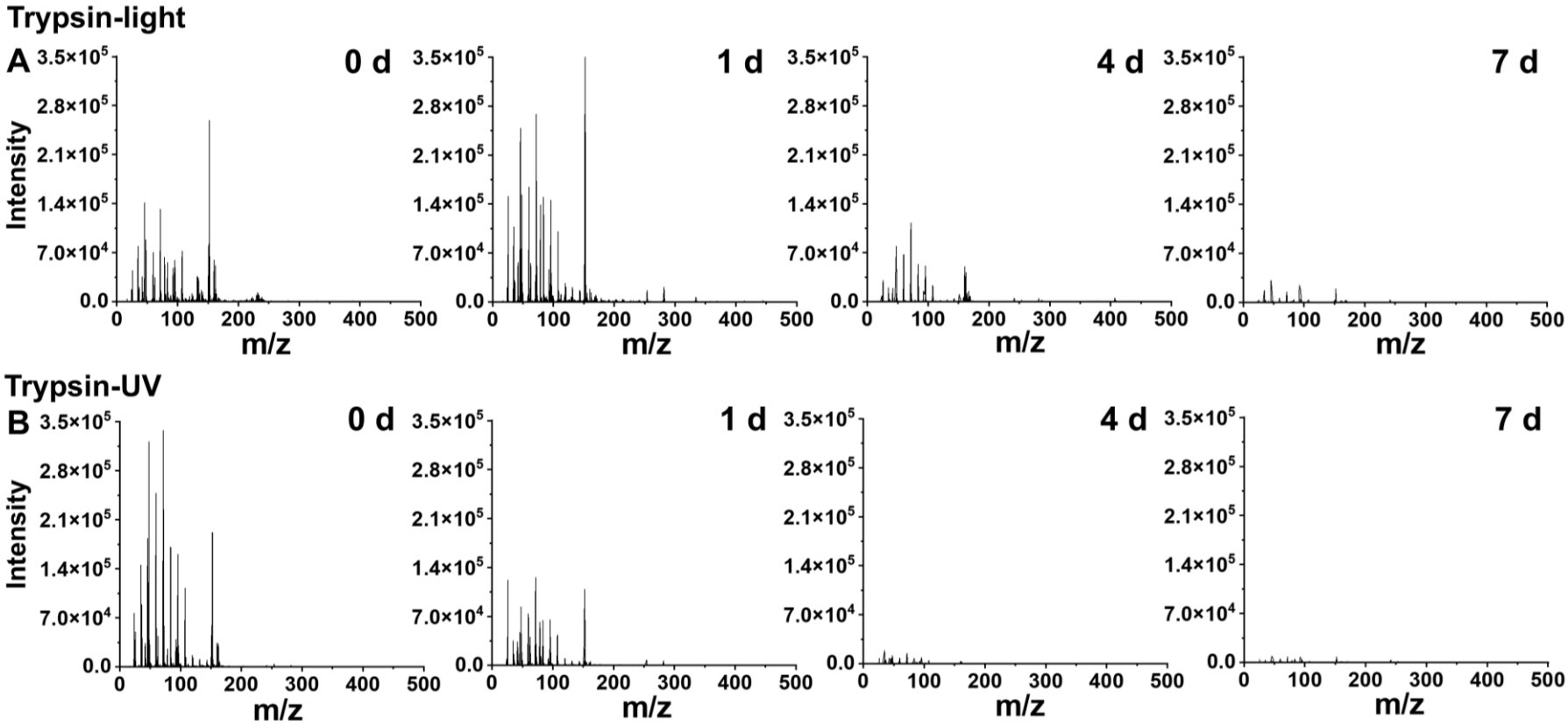

Figure S12. The effect of light on the degradation of MBFD induced by trypsin. A) Visible light and B) ultraviolet (UV) light. Under visible light, the peaks of MBFD and degradation clusters initially increased and then decreased over 0-7 days of incubation. Conversely, under UV light, the MBFD peaks gradually decreased, indicating degradation by trypsin. After 4 days of incubation, the MBFD peaks almost completely disappeared, suggesting complete degradation of MBFD. Comparing the results between UV and visible light, it was found that the degradation efficiency of MBFD under UV light was significantly higher than under visible light. This indicates that UV light might be the most effective for accelerating degradation. Incubation times were 0 day, 1 day, 4 days, and 7 days.

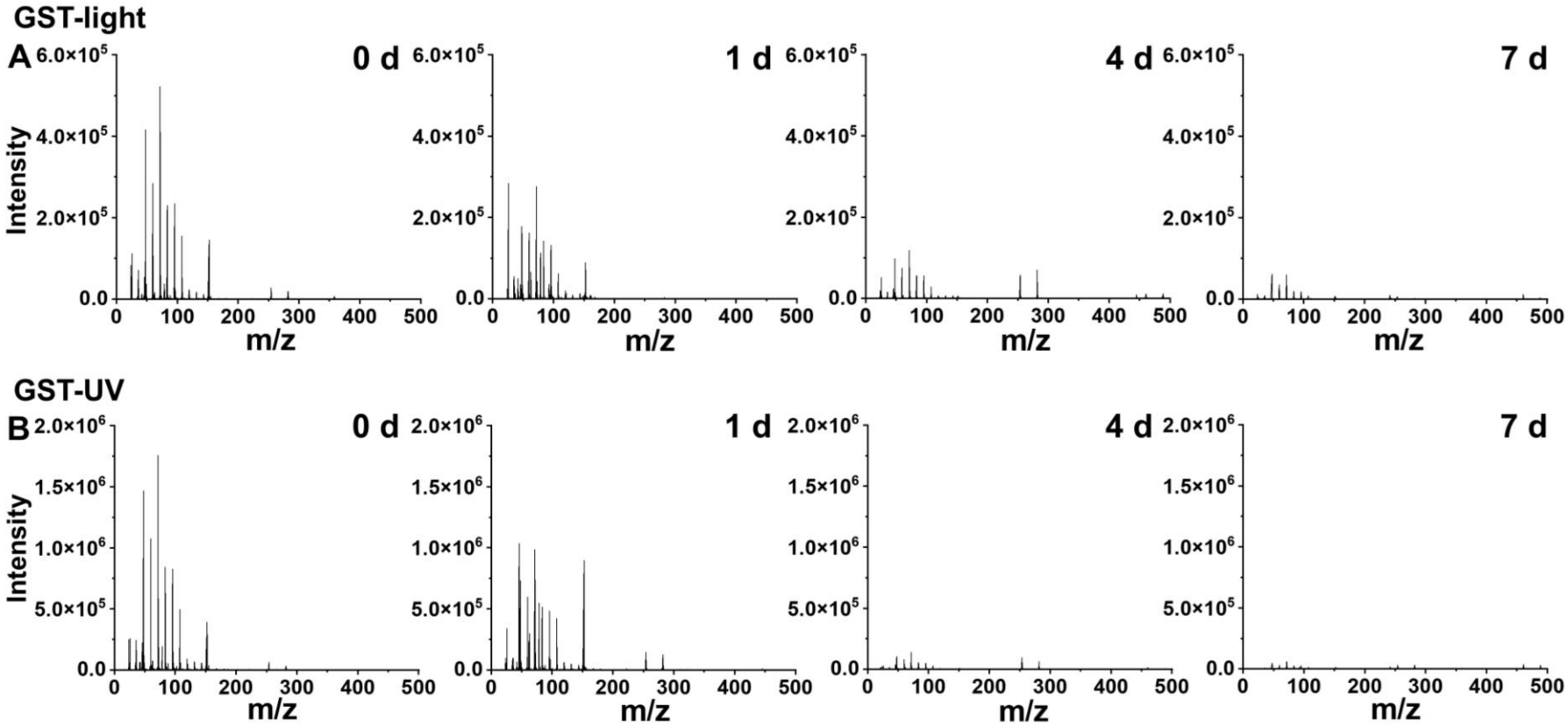

Figure S13. The effect of light on the degradation of MBFD induced by GST. A) Visible light and B) UV light. As the incubation period was extended from 0 to 7 days, a gradual decline in the typical peaks of MBFD and its degradation byproducts was observed. Notably, under identical experimental conditions, the peak intensities of MBFD demonstrated a marked reduction when exposed to light compared to those kept in darkness. These findings indicated that light exposure, particularly UV light, significantly enhanced the degradation rate of MBFD. Incubation time: 0 day, 1 day, 4 days, and 7 days.

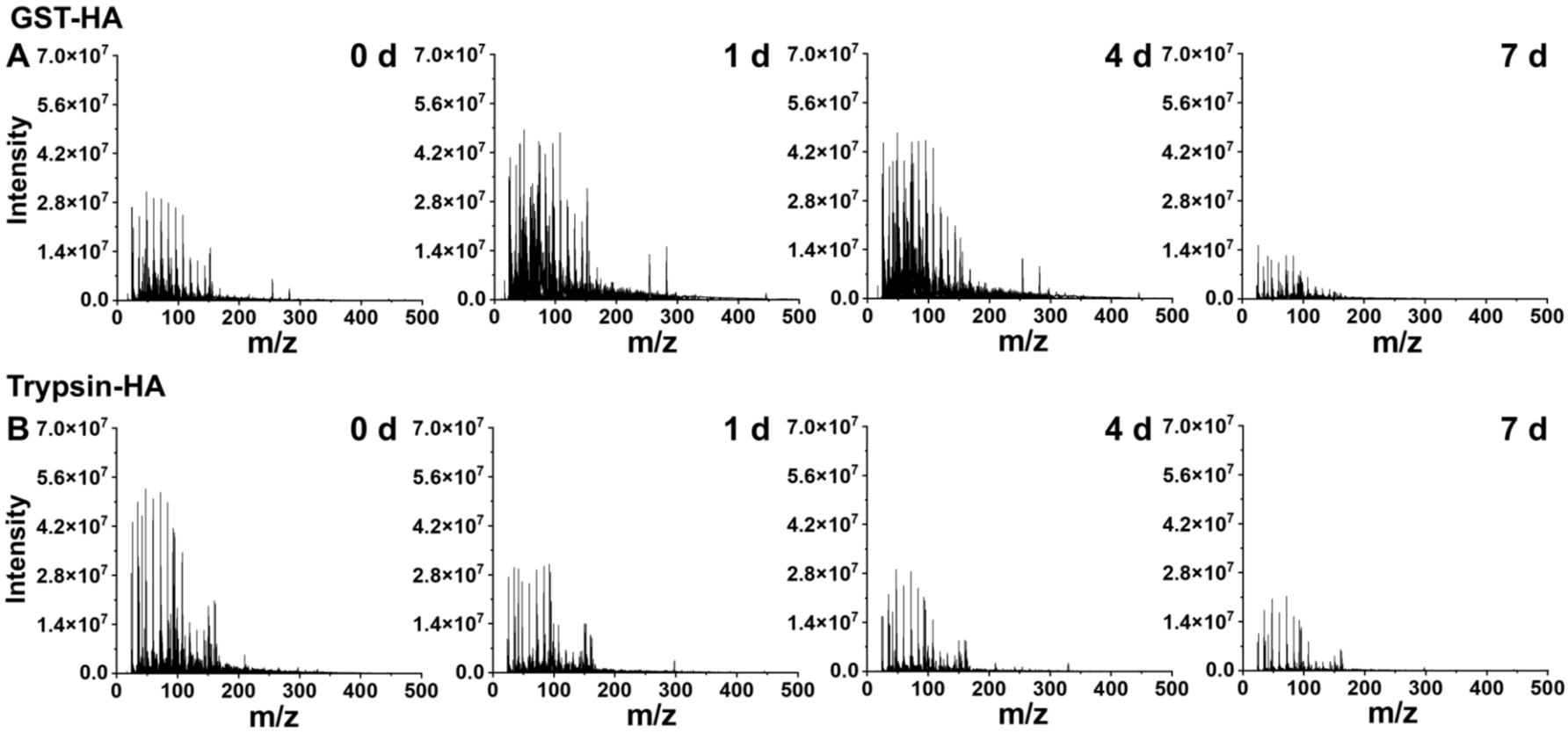

Figure S14. The effect of environmental matrices (HA) on the degradation of MBFD induced by A) GST and B) trypsin. It can be seen that prolonging the incubation time from 0 to 7 days, the typical peak of MBFD showed a decreasing trend, resembling the degradation trend observed in the absence of environmental matrices. During degradation, nitrogen- and oxygen-containing degradation products were produced. The types of products differed from those in water, indicating that different substrates influenced the type of degradation products. The concentration of humic acid (HA) was 1 mg/mL.

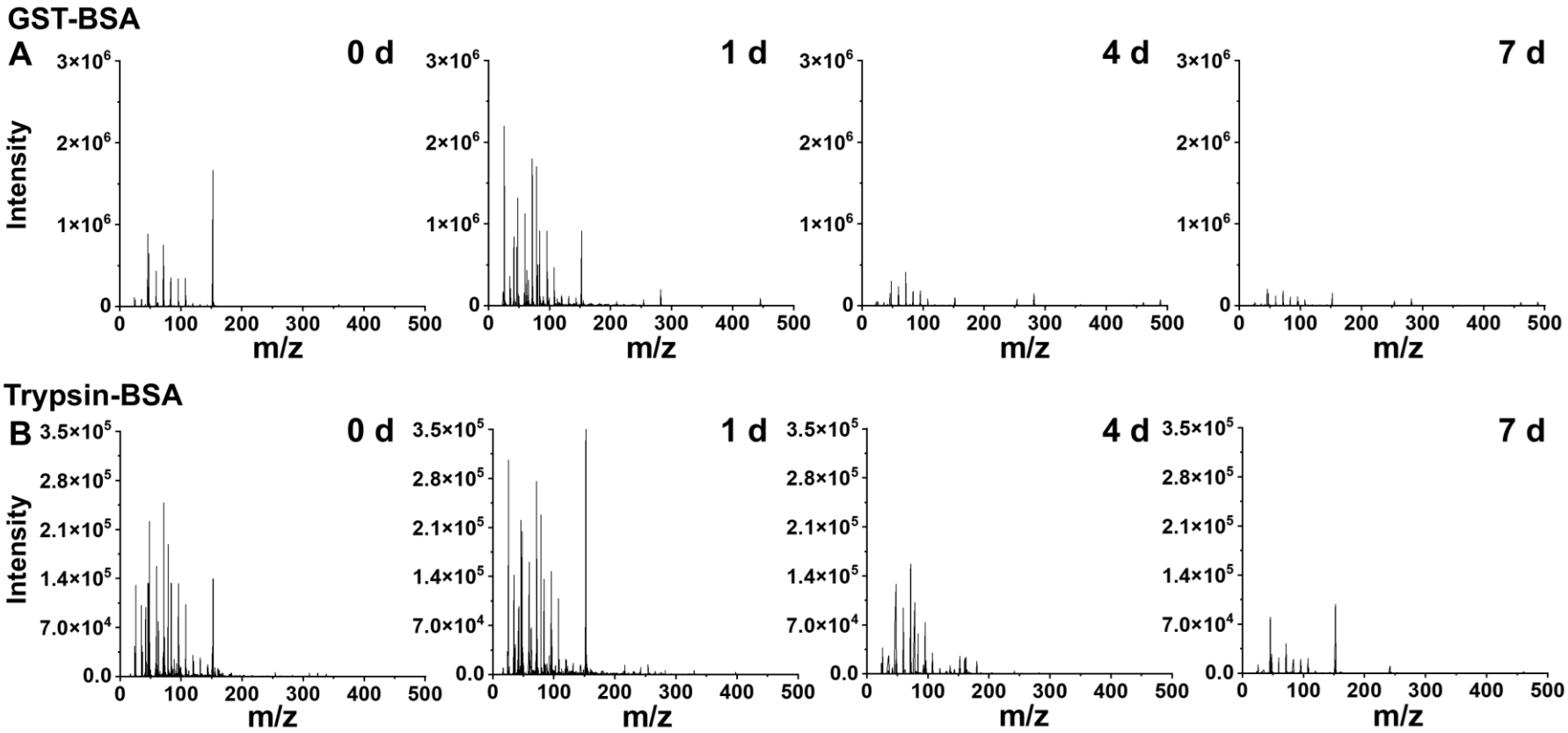

Figure S15. The effect of biological matrices (BSA) on A) GST and B) trypsin-induced degradation of MBFD. It can be seen that in the presence of BSA, the typical peaks were still observed with similar intensity, indicating that BSA did not interfere with the MS detection of MBFD. The typical peaks of MBFD exhibited a pattern of increase followed by decrease, resembling the degradation trend observed in the absence of a biological substrate. This suggests that MBFD can still undergo degradation by GST and trypsin even in the presence of BSA. The concentration of BSA was 1 μg/mL.

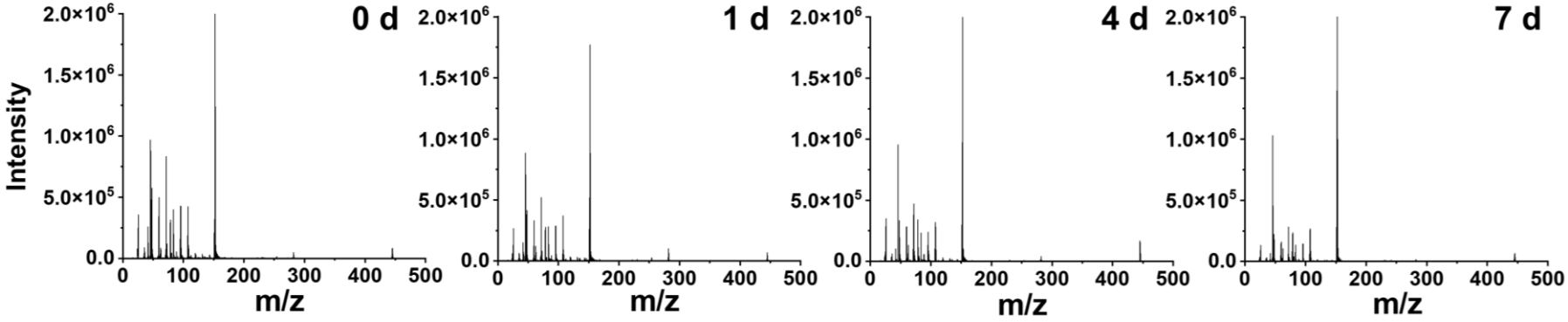

Figure S16. Mass spectra of MBFD in the presence of BSA. The results exhibited that the characteristic peaks of MBFD remained essentially unchanged over time, suggesting that BSA did not induce degradation of MBFD. This finding was also supported by the pattern of increase followed by decrease in the typical peaks of MBFD observed in the presence of enzyme and BSA, as illustrated in Fig. S15. The concentration of BSA was 1 μg/mL.

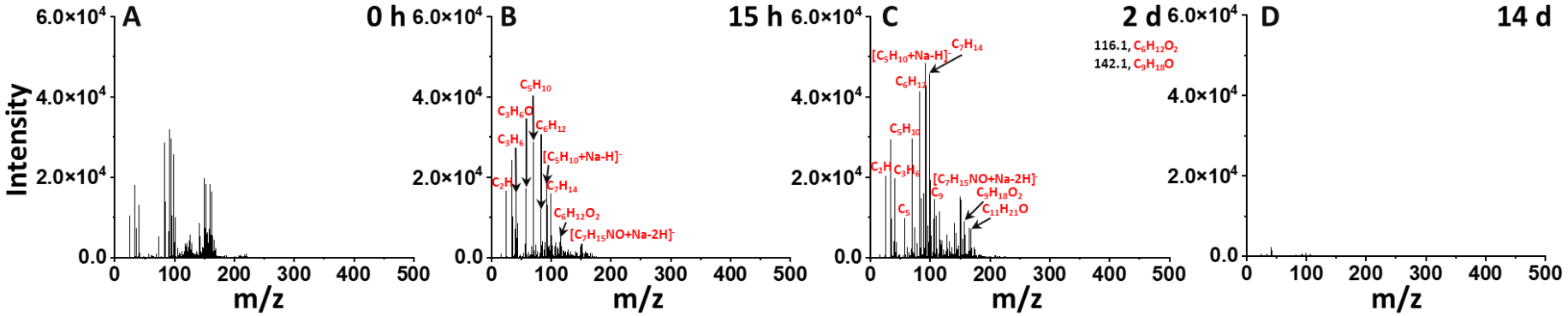

Figure S17. The effect of antioxidant 1010 on the trypsin-induced MBFD degradation by MS fingerprinting. Mass spectra of MBFD in the presence of trypsin and antioxidant 1010 (tetrakis[beta-(3,5-di-tert-butyl-4-hydroxyphenyl)propionic acid] pentaerythritol ester). Incubation time: A) 0 hour, B) 15 hours, C) 2 days, and D) 14 days. It can be seen that when incubation time was extended from 0 to 14 days with trypsin and antioxidant 1010, the MBFD peak initially increased and then decreased, similar to degradation without the antioxidant. This suggests that antioxidant 1010 does not impact MBFD degradation. The concentration of antioxidant 1010 was 50 μg/mL.

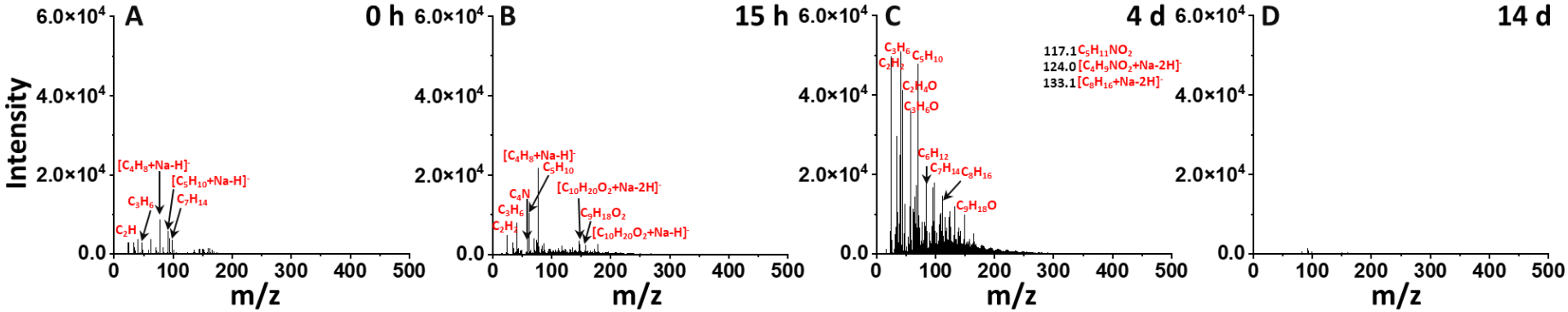

Figure S18. The effect of antioxidant 1010 on the GST-induced MBFD degradation by MS fingerprinting. Mass spectra of MBFD in the presence of GST and antioxidant 1010. Incubation time: A) 0 hour, B) 15 hours, C) 4 days, and D) 14 days. The concentration of antioxidant 1010 was 50 μg/mL.

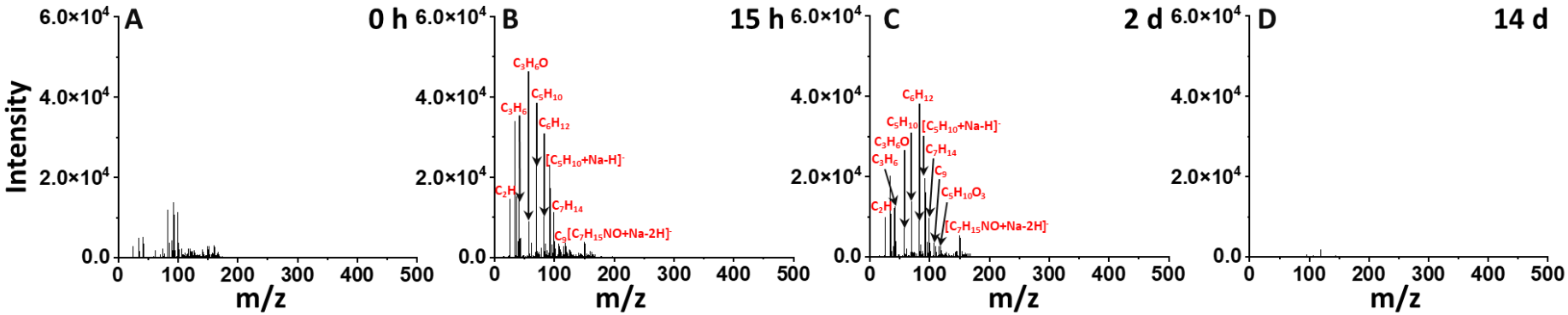

Figure S19. MS performance of MBFD degraded by trypsin in serum. Incubation time: A) 0 hour, B) 15 hours, C) 2 days, and D) 14 days. Prolonging the incubation time from 0 to 14 days, the typical peak of MBFD showed a trend of first increasing and then decreasing, similar to the degradation trend in water, indicating that MBFD can be degraded by trypsin in serum.

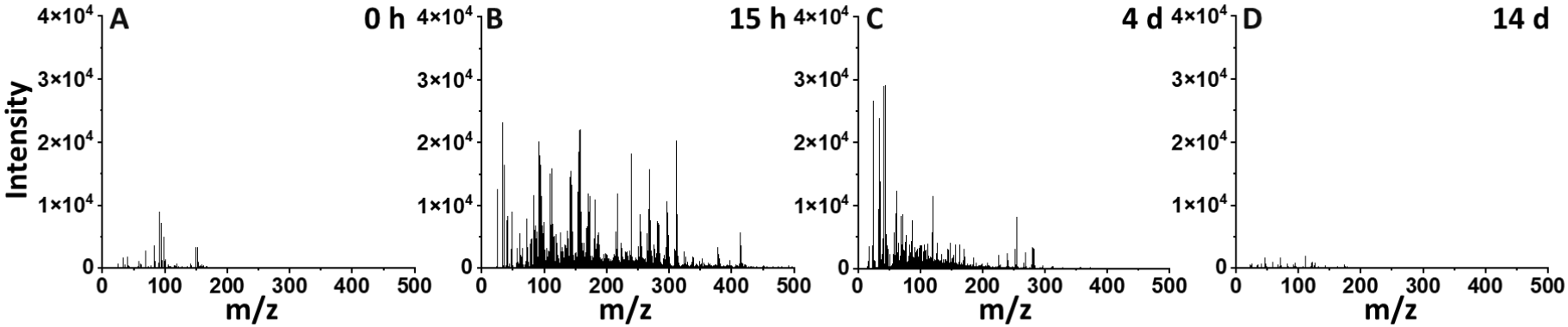

Figure S20. MS performance of MBFD degraded by GST in serum. Incubation time: A) 0 hour, B) 15 hours, C) 4 days, and D) 14 days. Prolonging the incubation time from 0 to 14 days, the typical peak of MBFD showed a trend of first increasing and then decreasing, similar to the degradation trend in water, indicating that MBFD can be degraded by GST in serum.

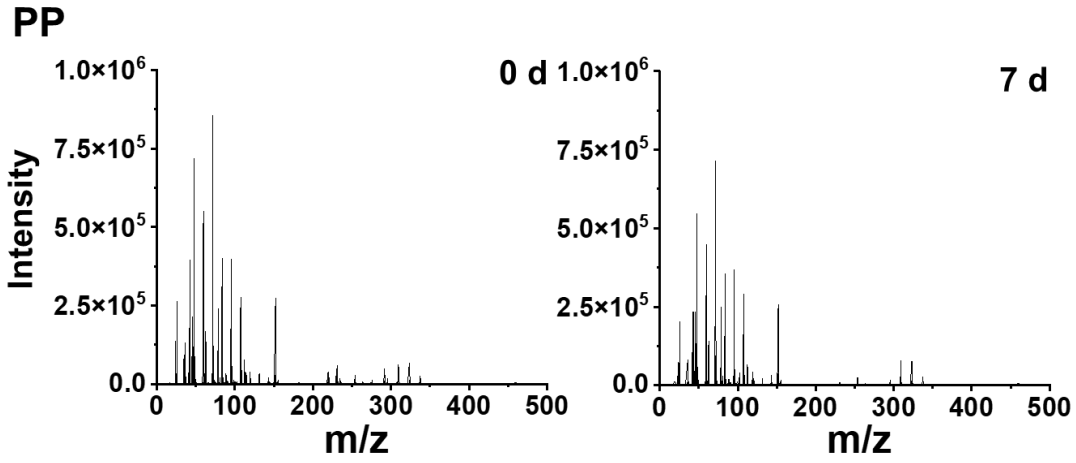

Figure S21. Mass spectra of PP industrial particles over time. After incubating 7 days, the typical peak of PP particles remained stable, indicating that PP particles did not degrade in the absence of enzymes.

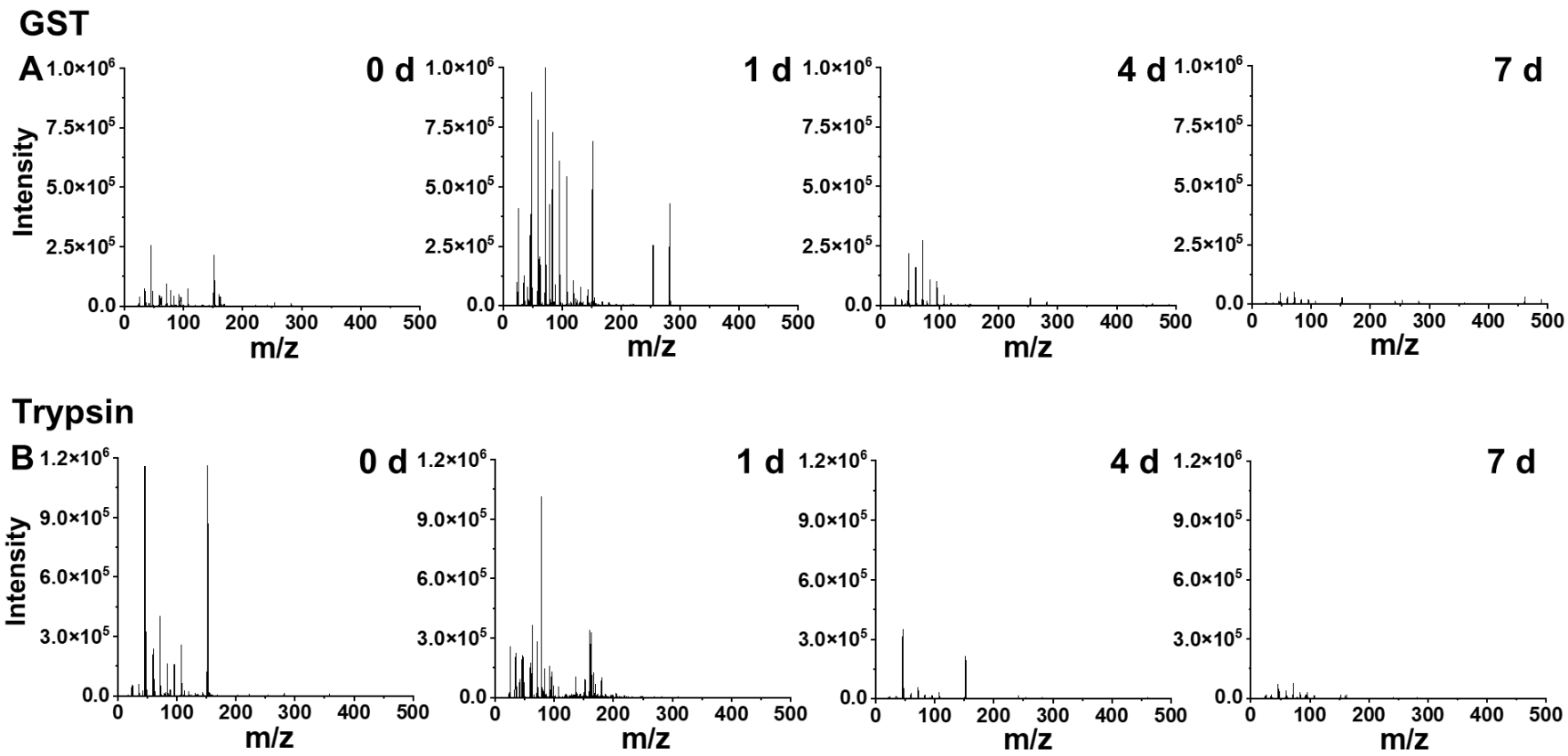

Figure S22. Mass spectra of MBFD of discarded disposable activated carbon masks in the presence of A) GST and B) trypsin. By extending the incubation time from 0 to 7 days, it can be seen that the typical peaks of MBFD and degradation clusters showed a trend of first increasing and then decreasing, indicating that GST and trypsin could also degrade disposable activated carbon masks. This result suggests that the enzymatic method is suitable for the biodegradation of different types of PP-based masks. The incubation times were 0 day, 1 day, 4 days, and 7 days.

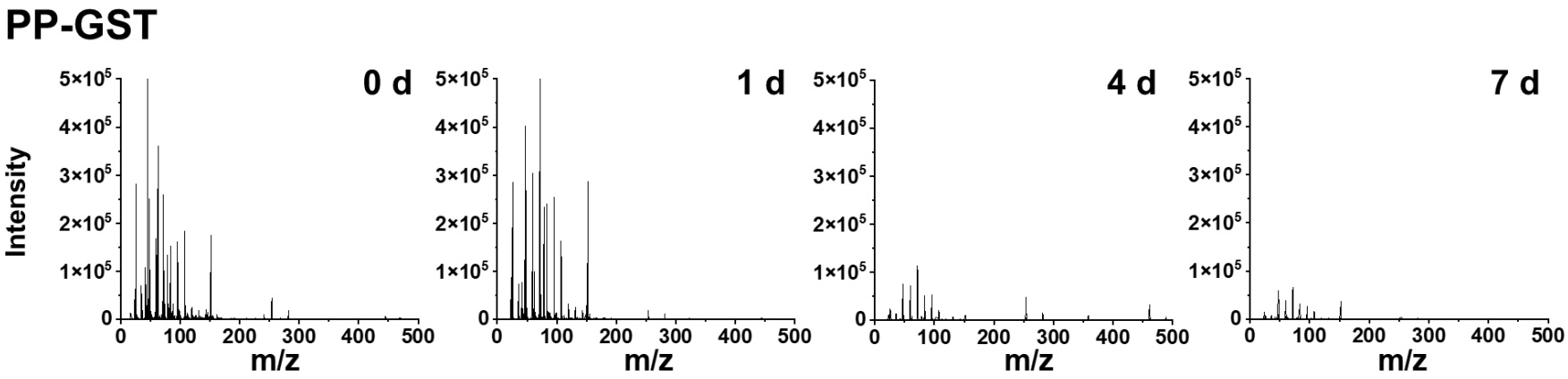

Figure S23. Mass spectra of PP industrial particles (100 kDa) in the presence of GST under dark condition. Over a 7-day incubation period, the peaks corresponding to PP particles initially increased and then decreased, indicating that the PP particles were degraded by the action of GST. This result showed a similar pattern to MBFD, suggesting that this enzymatic method was suitable for degrading different types of PP plastics.

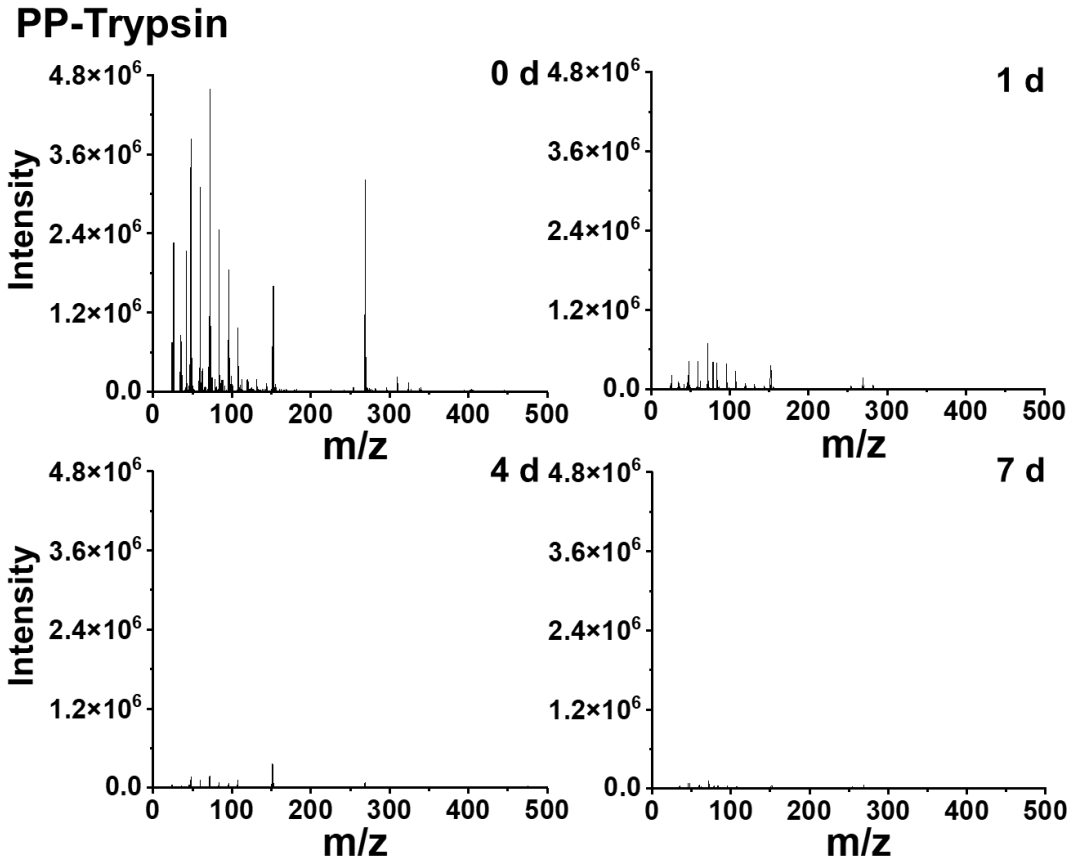

Figure S24. Mass spectra of PP industrial particles in the presence of trypsin under dark condition. Extending the incubation time from 0 to 7 days resulted in a decrease in the typical peak of PP particles, suggesting that the PP particles were degraded by trypsin. This result demonstrates the effectiveness of this enzymatic approach for various types of PP plastics.

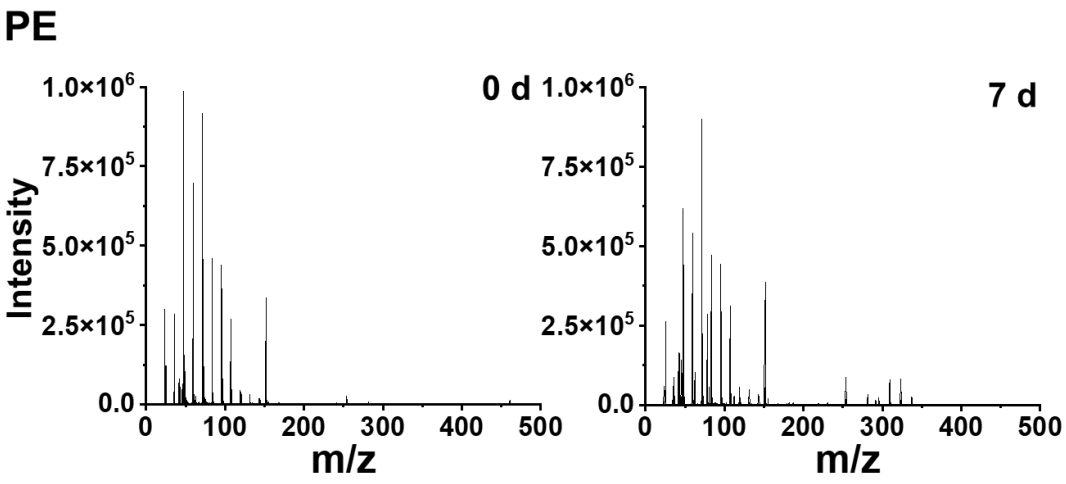

Figure S25. Mass spectra of polyethylene (PE) particles over time. The peak corresponding to PE particles remained consistent after 7 days of incubation. This indicates that PE particles do not degrade in the absence of enzymes.

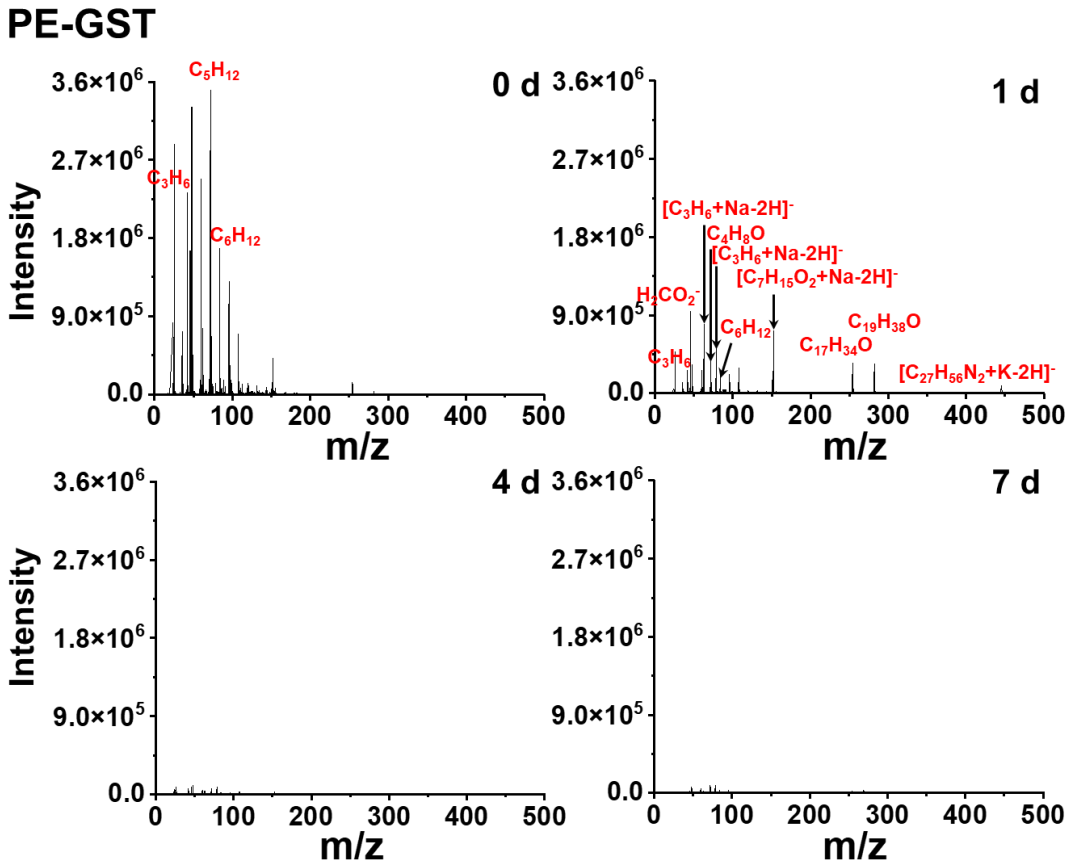

Figure S26. Mass spectra of PE particles in the presence of GST. It was observed that under dark conditions, PE particles could be degraded by GST, leading to a significant decrease in the typical peak of PE particles. This degradation process produced degradation products containing nitrogen and oxygen, which differed somewhat from the products of PP particles.

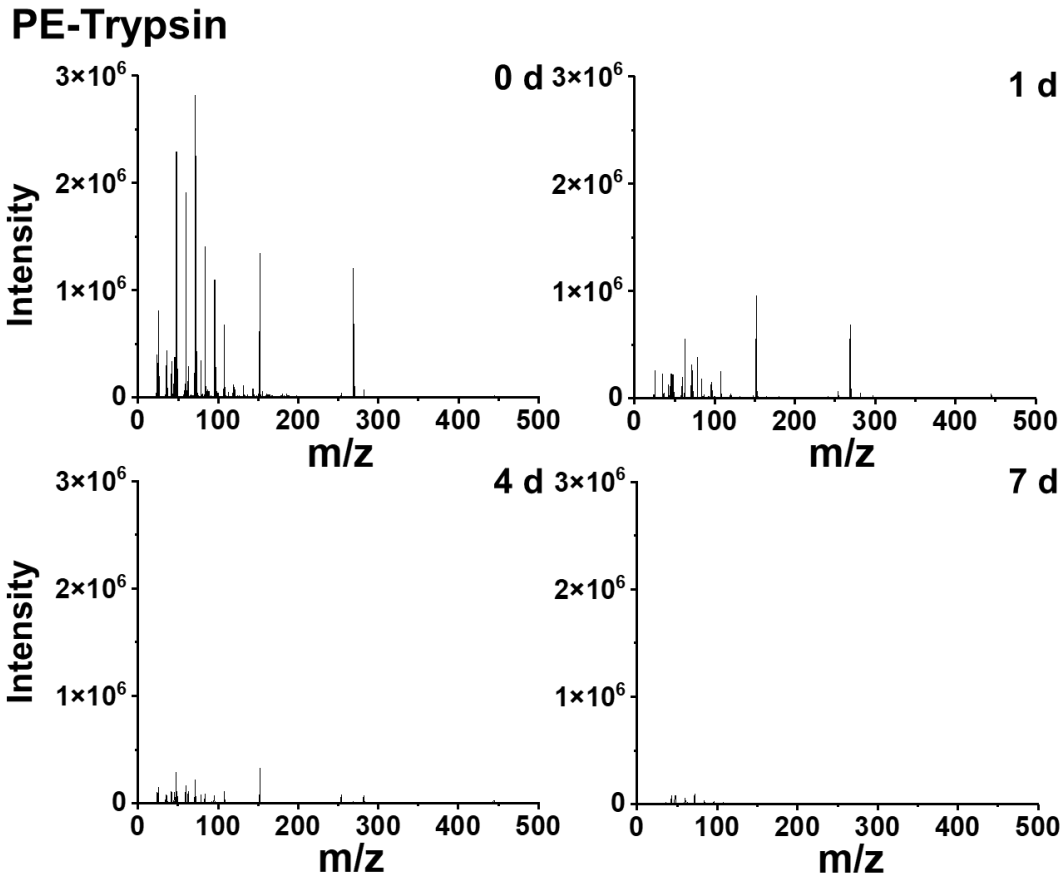

Figure S27. Mass spectra of PE particles in the presence of trypsin. The results indicated that trypsin could degrade PE particles, resulting in a decrease in the characteristic peak of PE particles.

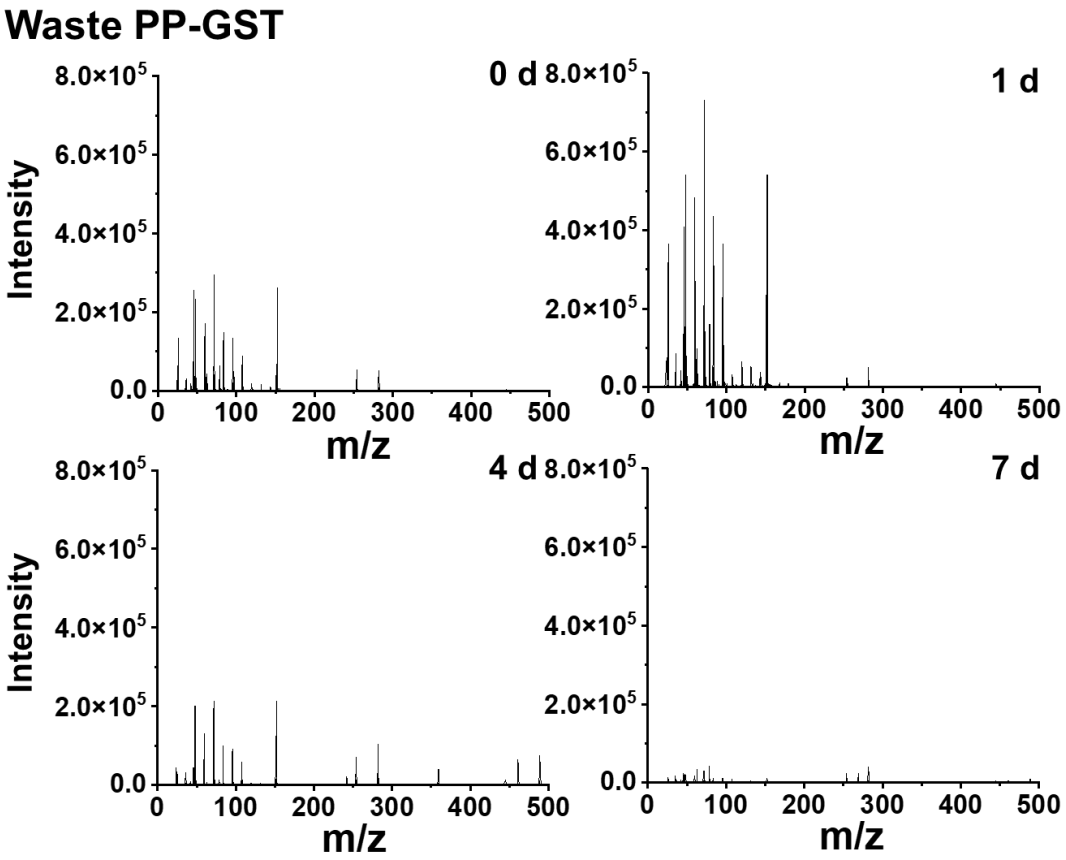

Figure S28. MS fingerprinting of PP industrial particles in the wastewater treated with GST. The characteristic peak of PP particles exhibited a pattern of initially increasing and then decreasing, mirroring the degradation trend observed in MBFD over time. These findings indicated that GST had the ability to degrade PP industrial particles, making it a promising tool for plastic treatment.

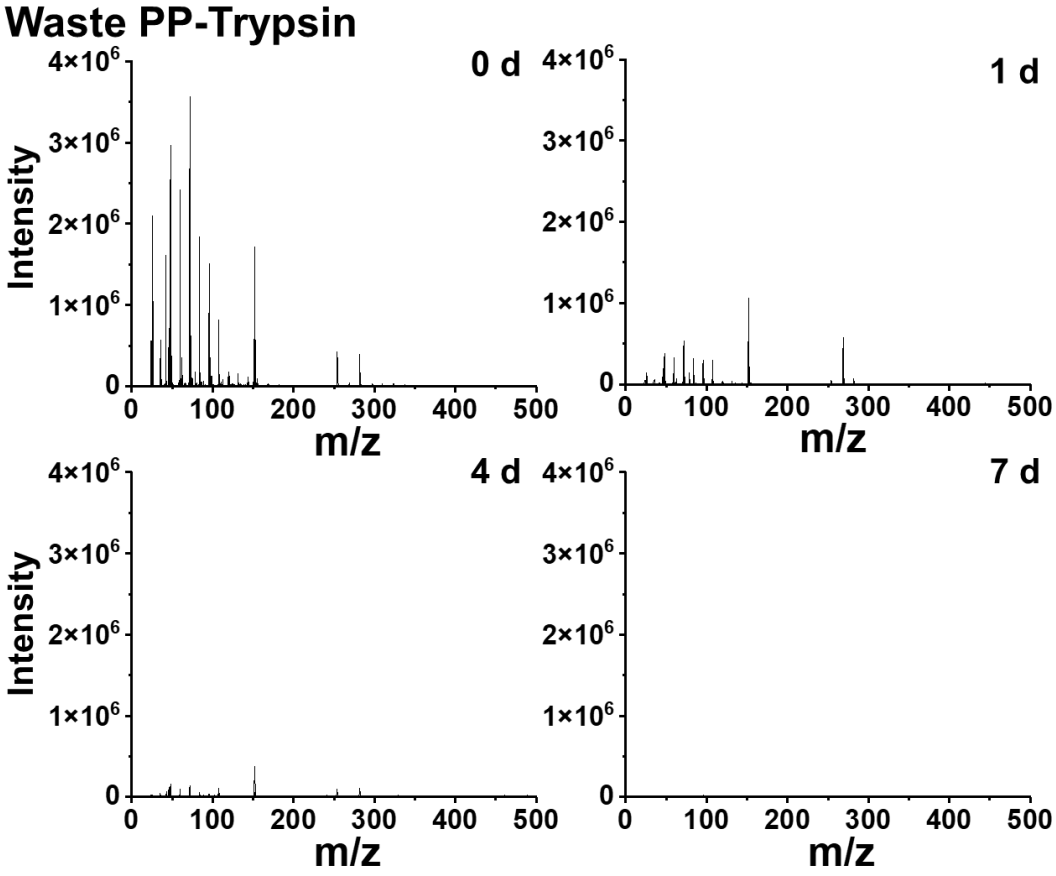

Figure S29. Mass spectra of PP industrial particles in the wastewater treated with trypsin. Extending the incubation period from 0 to 7 days resulted in a decrease in the typical peak of PP particles, indicating that trypsin had the ability to degrade industrial PP particles in wastewater. This result demonstrated the potential for practical plastic treatment.

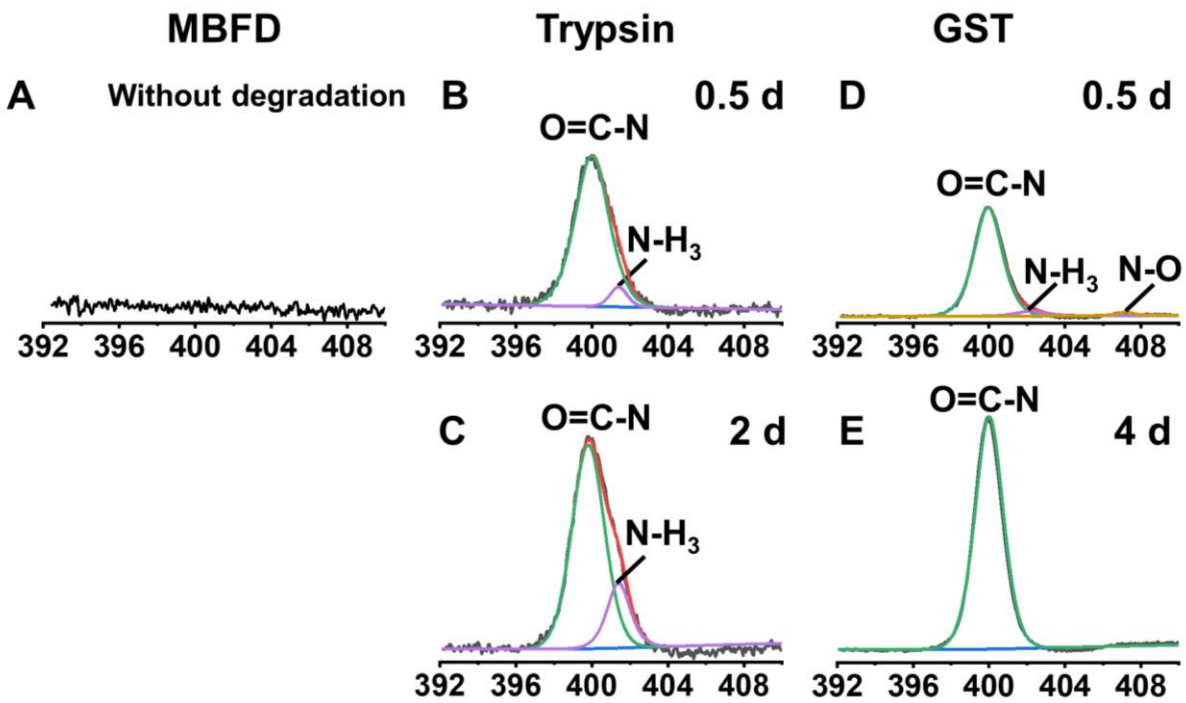

200

201 **Figure S30. The N1 XPS spectra of MBFD treated with enzymes over time.** A) Without
202 degradation, (B-C) degradation under dark conditions (37 °C) by trypsin; (D-E) degradation
203 under dark conditions (37 °C) by GST. The incubation time was (B, D) 0.5 d, C) 2 d, and E) 4
204 d, respectively. The -O=C-N-, -N-H-, and -N-O-bonds in MBFD yielded and progressively
205 increased with time following degradation, as can be observed in the N1 XPS spectra,
206 indicating the formation of the key oxidation and nitrided products.

207

208

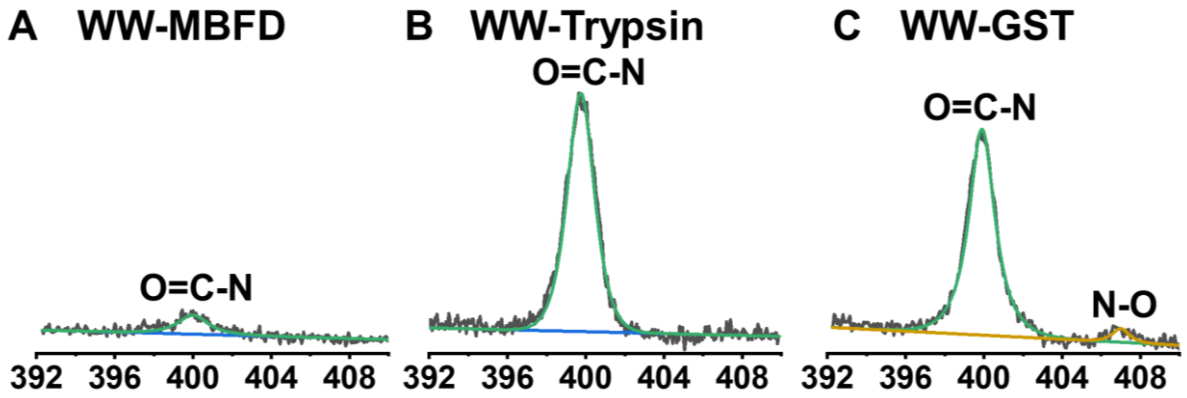

Figure S31. The N1 XPS spectra of MBFD in wastewater (WW) samples that were enzymatically degraded in a dark environment at 37 °C. A) Without degradation, B) MBFD degradation under dark conditions (37 °C) by trypsin; C) MBFD degradation under dark conditions (37 °C) by GST. The peaks of the -O=C-N- and -N-O- bonds in MBFD increased following degradation, according to the N1 XPS spectra, showing the formation of the oxidation and nitrided products.

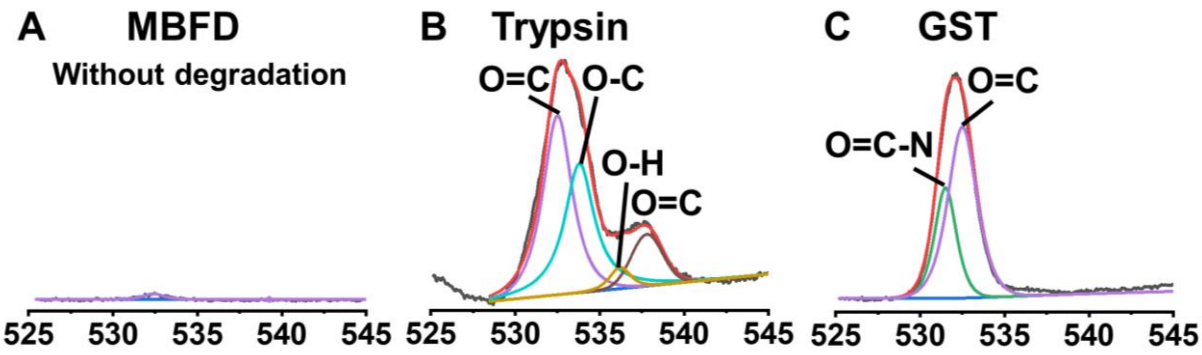

Figure S32. The O1 XPS spectra of MBFD treated with enzymes. A) Without degradation, B) degradation under dark conditions (37 °C) by trypsin; C) degradation under dark conditions (37 °C) by GST. MBFD had the peaks of -O=C-, -O=C-N-, -O-C-, and -O-H- bonds in the O1 XPS spectra following the biodegradation of trypsin and GST. These peaks indicated the formation of the oxidation and nitrided products.

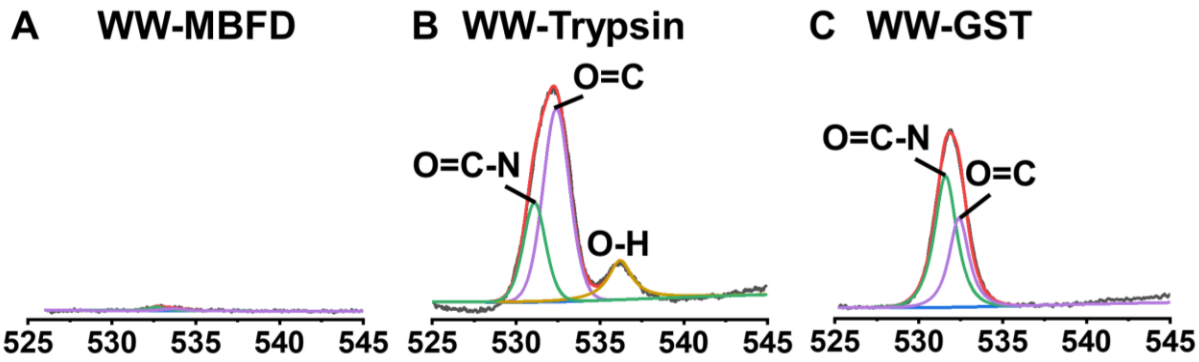

Figure S33. The O1 XPS spectra of MBFD treated with enzymes. A) Without degradation, B) MBFD in wastewater (WW) samples under dark conditions (37 °C) degraded by trypsin; C) MBFD in wastewater (WW) samples under dark conditions (37 °C) degraded by GST. The peaks of the -O=C-N-, -O=C-, and -O-H- bonds during enzyme-induced degradation were indicative of the formation of the oxidation and nitrided products, according to the O1 XPS spectra.

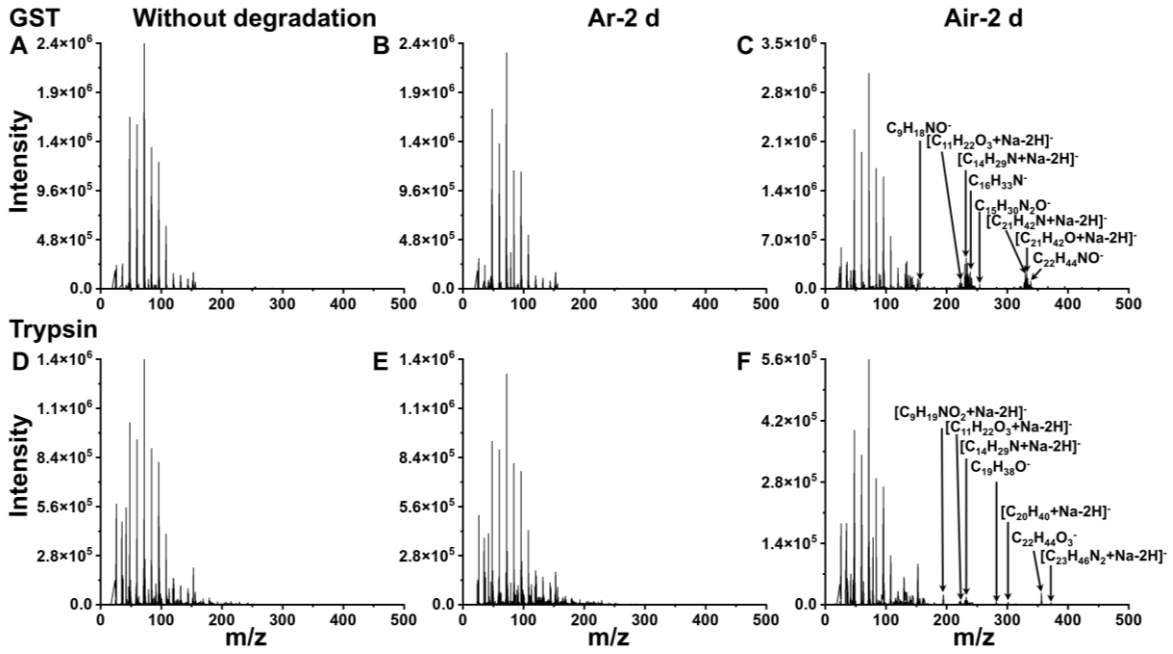

Figure S34. Comparison of mass spectra of the degradation of MBFD induced by GST (A-C) and trypsin (D-F) using Ar gas as a protective environment and in the presence of air. (A, D) Without degradation, (B, E) incubation for 2 days with Ar gas, (C, F) incubation for 2 days in the presence of air. Almost no peaks corresponding to N- and O-containing products were obtained after 2 days of incubation with Ar gas. However, in the presence of air (nitrogen and oxygen), the peaks of N- and O-containing degradation products gradually increased. These results suggest that MBFD can be degraded by GST and trypsin, and the N and O in the degradation products originate from the air dissolved in the solution, thus supporting the molecular mechanisms in Figure 4.

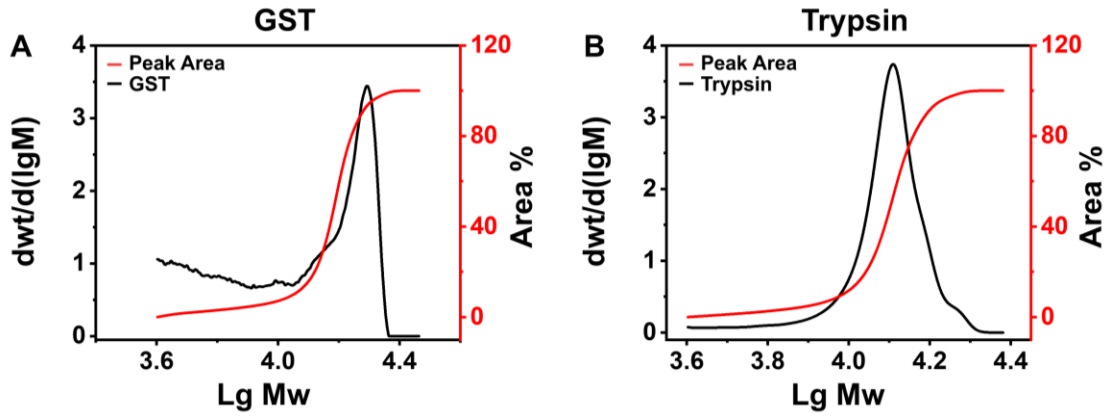

Figure S35. Gel permeation chromatography (GPC) analysis was conducted on GST and trypsin. The figure displays the molecular weight distribution (MWD) of the enzymes analyzed through GPC. The polydispersity index of Mw/Mn was 1.15 and 1.03, respectively, which was consistent with a narrow MW distribution (Mw/Mn < 1.20) of biological macromolecular proteins.[1-5] Besides, the GPC analysis results only showed peaks for GST and trypsin, with no peaks detected for other proteins. This confirms that neither GST nor trypsin have any carry-over proteins that can impact their degradation activity.

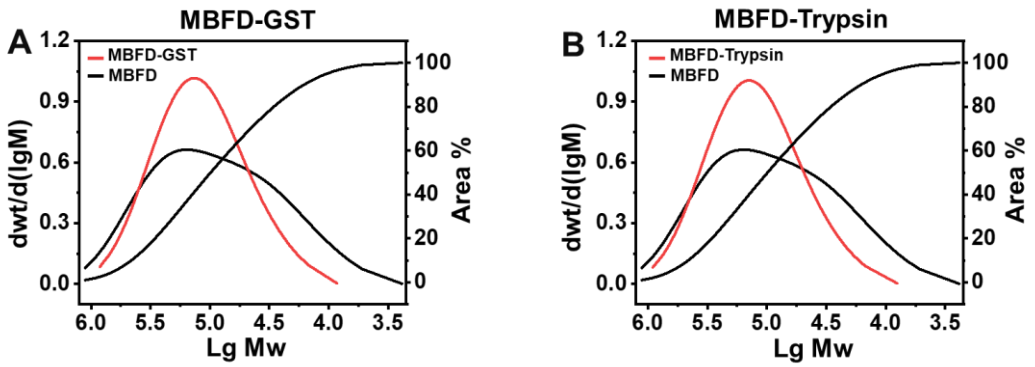

Figure S36. GPC analysis of MBFD after 1 day of reaction catalyzed by GST and trypsin. This figure compares the reactions with and without these enzymes. It specifically shows the GPC analysis of MBFD degraded by A) GST and B) trypsin.

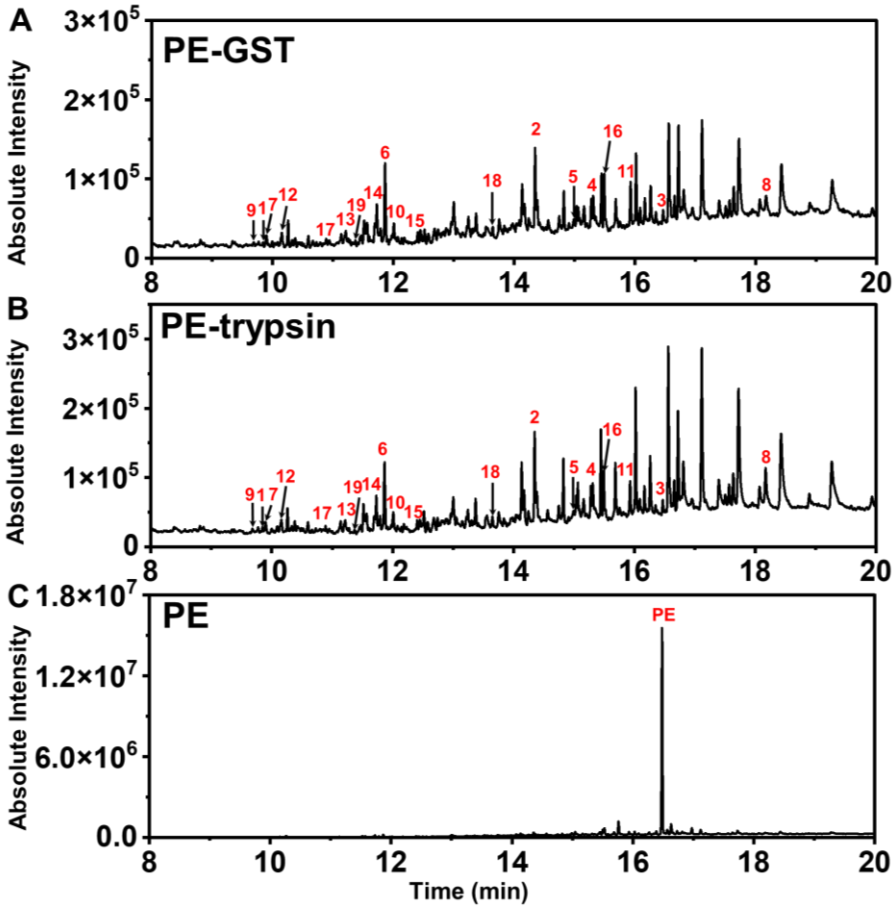

Figure S37. TIC diagram of PE particles obtained using GC-MS. Following the degradation, the PE plastics treated with trypsin and GST showed characteristic peaks at specific retention times of 9.846, 14.352, 16.467, 15.310, 14.989, 11.865, 9.897, 18.172, 9.682, 12.011, 15.929, 10.155, 11.213, 11.729, 12.405, 15.492, 10.888, 13.558, and 11.371 minutes. Simultaneously, the PE particles without GST and trypsin degradation exhibited a distinct peak at a retention time of 16.482 minutes. Mass spectrometry was then employed to analyze the components detected in the aforementioned retention time peaks. The results indicated that the degradation products of PE included "Oxalic acid, 2-ethylhexyl hexyl ester" (1), "n-Hexadecanoic acid" (2), "Phenol,2,2'-methylenebis[6-(1,1-dimethylethyl)-4-methyl" (3), "Octadecanoic acid" (4), "Eicosyl nonyl ether" (5), "2, 4-di-tert-butylphenol" (6), "Benzaldehyde" (7), "13-Docosenamide" (8), "Dodecane" (9), "Pentadecane" (10), "Tetracosane" (11), "Tridecane" (12), "Nonadecane" (13), "Hexadecane" (14), "Heneicosane" (15), "Eicosane" (16), "2-dimethyldodecane" (17), "Octacosane" (18), and "Heptadecane" (19) (see in Table S3). All these compounds have high matching scores (over 80%) in the NIST library. The results indicated that the degradation products of PE degraded by GST and trypsin included oxygen-containing compounds, nitrogen-containing compounds, and hydrocarbons. The presence of nitrided and oxidation products validated the reliability of our findings.

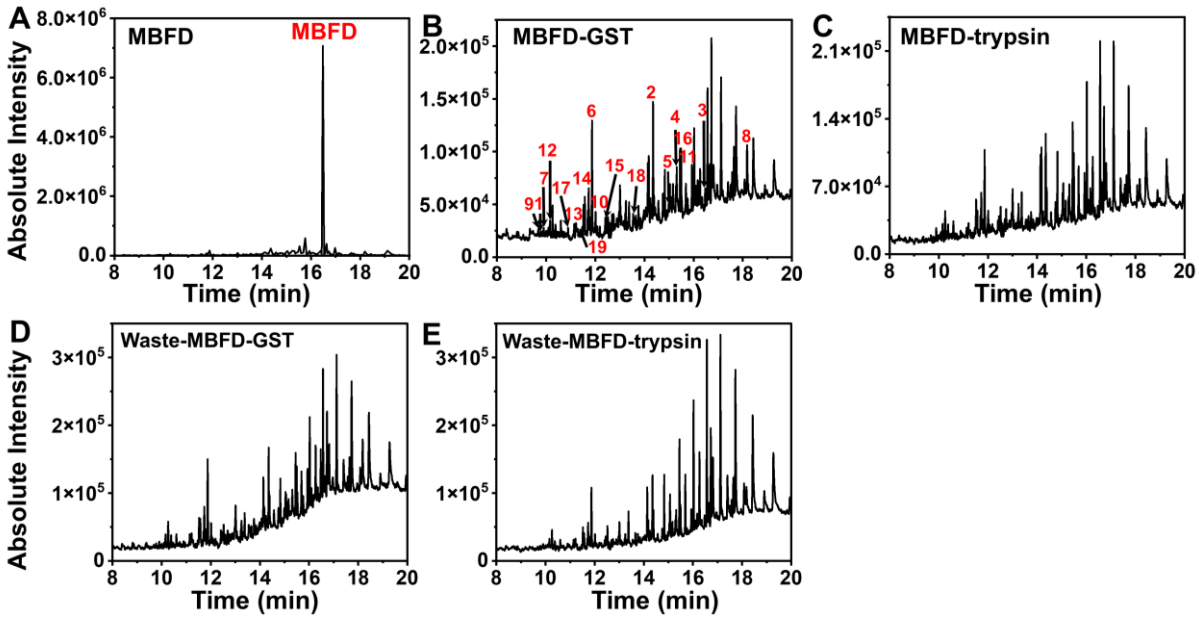

Figure S38. TIC diagram of MBFD and its degradation products degraded by trypsin and GST. TIC diagram of degradation products of PP-based MBFD in 7 days. The MBFD substrate, which was not degraded by GST and trypsin, exhibited characteristic peaks at a retention time of 16.481 minutes. This retention time closely matched that of PE, suggesting that GC-MS was unable to differentiate between PE and PP-based MBFD due to their similar properties. Following the degradation, the products of PP-based MBFD treated with trypsin and GST were similar to those of PE plastics. This suggests that the degradation products of GST and trypsin on PP-based MBFD included oxygen-containing compounds, nitrogen-containing compounds, and hydrocarbons.

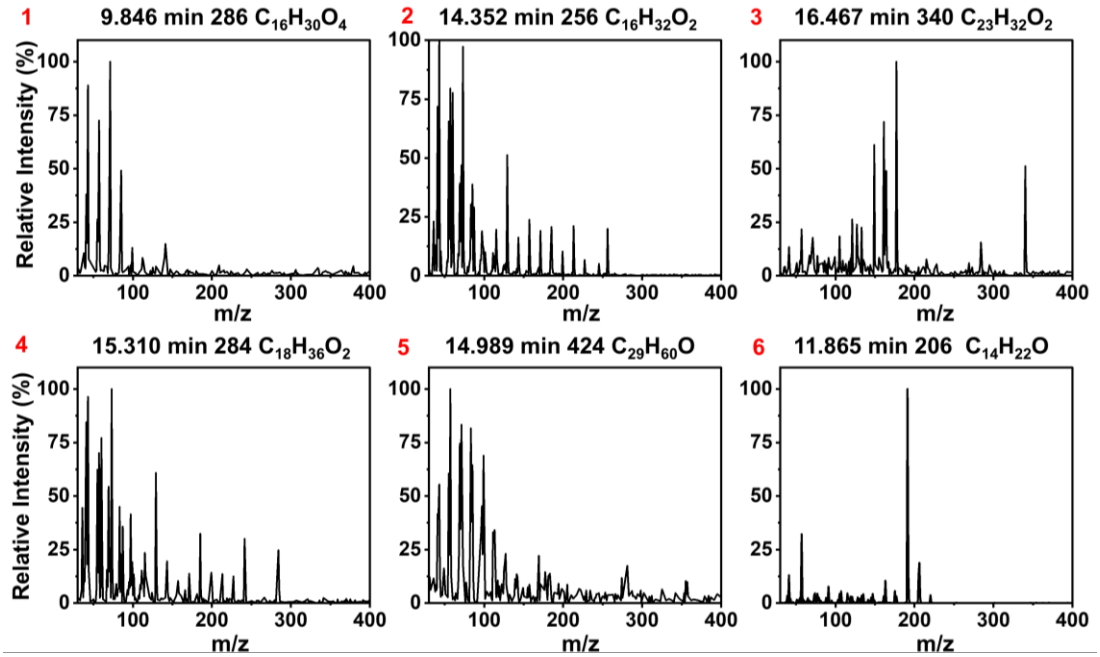

Figure S39. MS analysis of degradation products of MBFD and PE degraded by trypsin and GST. It includes mass spectra and molecular formulas of potential degradation products 1 to 6 of MBFD and PE, corresponding to the degradation products in TIC diagrams 1 to 6 in Fig. S37 and S38. The results indicated that the degradation products of MBFD and PE contained oxygen-containing compounds.

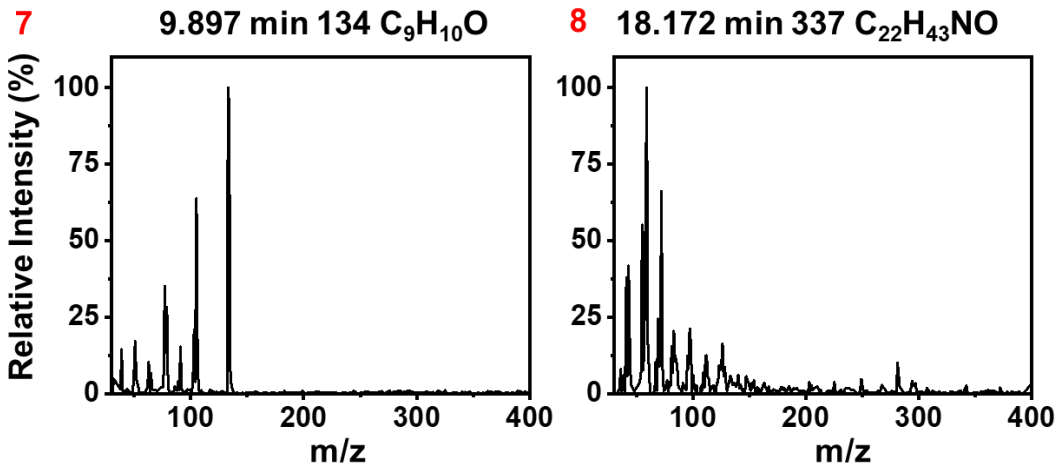

Figure S40. MS analysis of degradation products of MBFD and PE degraded by trypsin and GST. The figure displays mass spectra and molecular formulas of potential degradation products, corresponding to those in TIC diagrams 7 and 8 in Fig. S37 and S38. It can be seen that the degradation products of GST and trypsin on PP-based MBFD and PE contained oxygen and nitrogen-containing compounds.

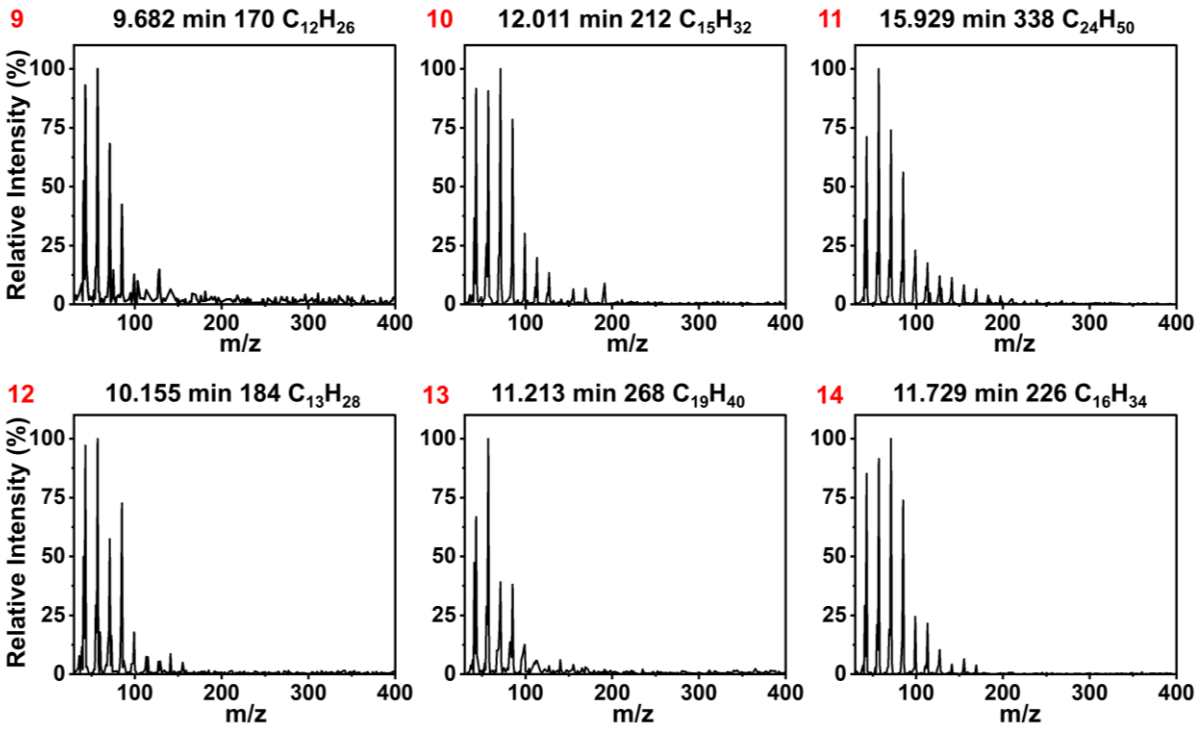

Figure S41. MS analysis of degradation products of MBFD and PE degraded by trypsin and GST. The figure displays mass spectra and molecular formulas of potential degradation products, corresponding to those in TIC diagrams 9 to 14 in Fig. S37 and S38. It can be seen that hydrocarbons were among the degradation products of trypsin and GST on PP-based MBFD and PE.

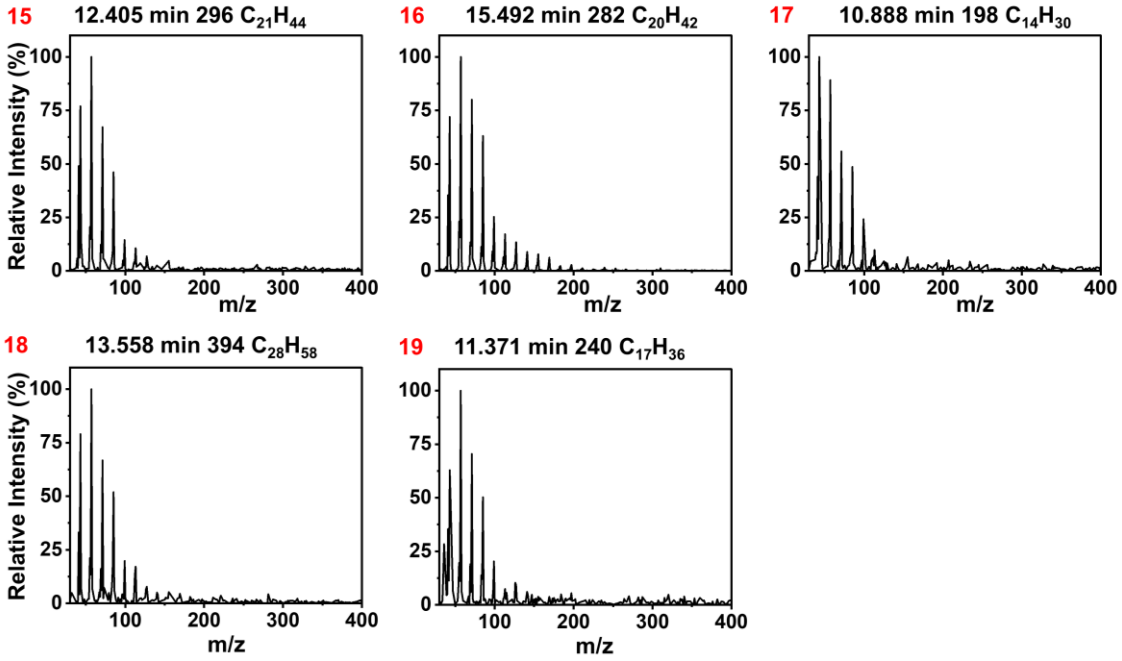

Figure S42. MS analysis of degradation products of MBFD and PE resulting from trypsin and GST degradation. The figure shows mass spectra and molecular formulas of potential degradation products, corresponding to those in TIC diagrams 15 to 19 in Figures S37 and S38. It is evident that hydrocarbons were identified as degradation products of trypsin and GST on PP-based MBFD and PE.

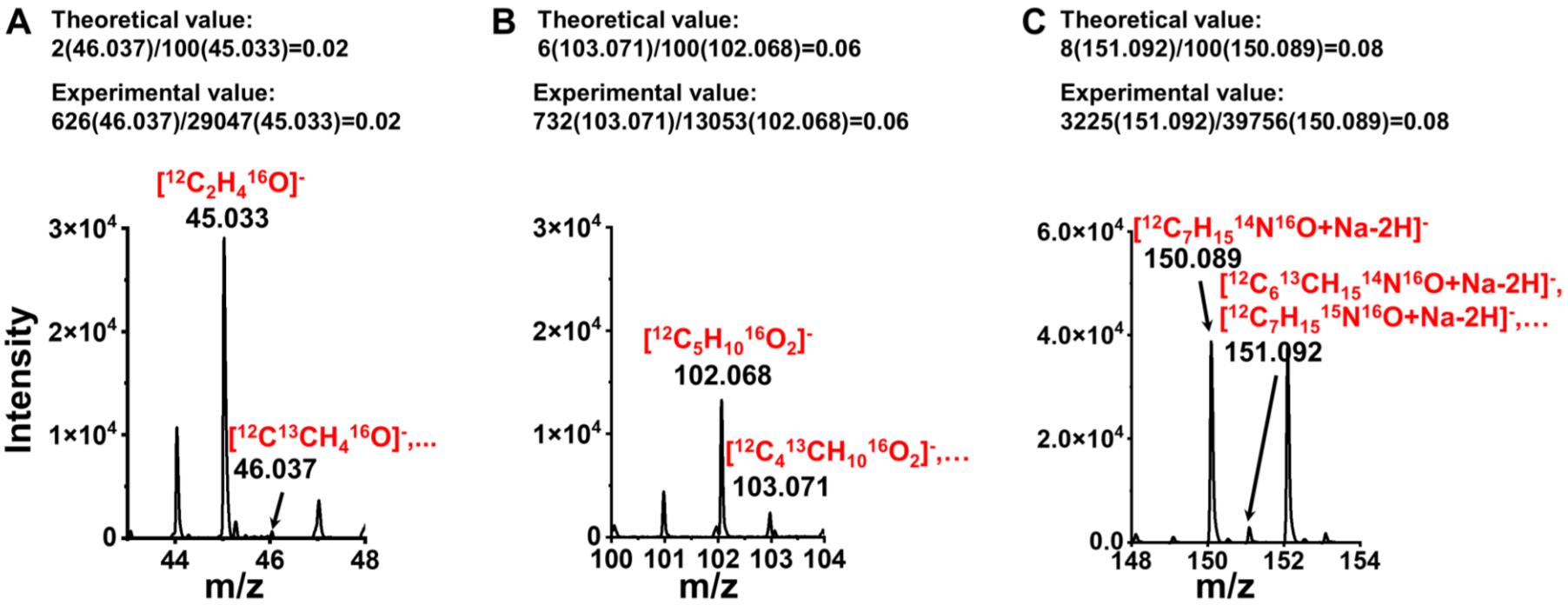

Figure S43. The stable isotope patterns of carbon and nitrogen isotope patterns confirming the nitrided products and oxidation products during trypsin-induced MBFD degradation. Three nitrided and oxidation products ($[C_2H_4O]^-$, $[C_5H_{10}O_2]^-$, and $[C_7H_{15}NO+Na-2H]^-$) in negative-ion LDI-TOF MS were visible as peaks in the mass spectra. Two naturally occurring stable isotopes of nitrogen (^{14}N and ^{15}N) have an abundance ratio of 99.634%:0.366%, while two naturally occurring stable isotopes of carbon (^{12}C and ^{13}C) have an abundance ratio of 98.893%:1.107%. For the nitrided products (*i.e.*, $[^{12}C_6{}^{13}CH_{15}{}^{14}N{}^{16}O+Na-2H]^-$ and $[^{12}C_7H_{15}{}^{15}N{}^{16}O+Na-2H]^-$), the measured values of the stable C and N isotope patterns agreed well with the theoretical values. Furthermore, the experimental values of the stable C isotope patterns for oxidation products ($[^{12}C{}^{13}CH_4{}^{16}O]^-$ and $[^{12}C_4{}^{13}CH_{10}{}^{16}O_2]^-$) were likewise maintained with the theoretical values, suggesting oxidation products were produced during the degradation process.

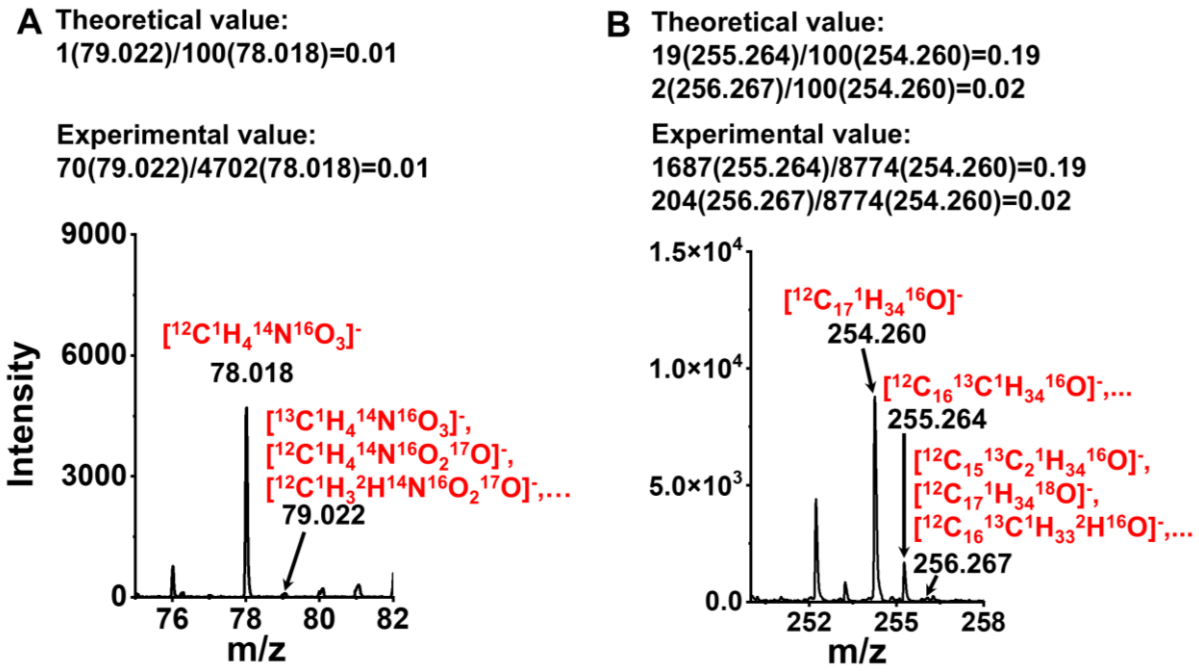

Figure S44. The stable isotope patterns of carbon and oxygen confirming the oxidation products during the GST-induced MBFD degradation. Two oxidation products ($[C_{17}H_{34}O]^-$ and $[CH_4NO_3]^-$) in negative-ion LDI-TOF MS are seen as peaks in the mass spectra. There are three naturally occurring stable isotopes of oxygen (^{16}O:^{17}O:^{18}O, 99.763%:0.038%:0.200%), compared to two naturally occurring stable isotopes of carbon (^{12}C and ^{13}C) with an abundance ratio of 98.893%:1.107%. For the oxidation products, namely $[^{12}C_{16}{}^{13}C^{1}H_{34}{}^{16}O]^-$, $[^{12}C_{15}{}^{13}C_2{}^{1}H_{34}{}^{16}O]^-$, $[^{12}C_{17}{}^{1}H_{34}{}^{18}O]^-$, $[^{12}C_{16}{}^{13}C^{1}H_{33}{}^{2}H^{16}O]^-$, $[^{13}C^{1}H_4{}^{14}N^{16}O_3]^-$, $[^{12}C^{1}H_4{}^{14}N^{16}O_2{}^{17}O]^-$, and $[^{12}C^{1}H_3{}^{2}H^{14}N^{16}O_2{}^{17}O]^-$, the experimental values of the stable C and O isotope patterns were in agreement with the theoretical values.

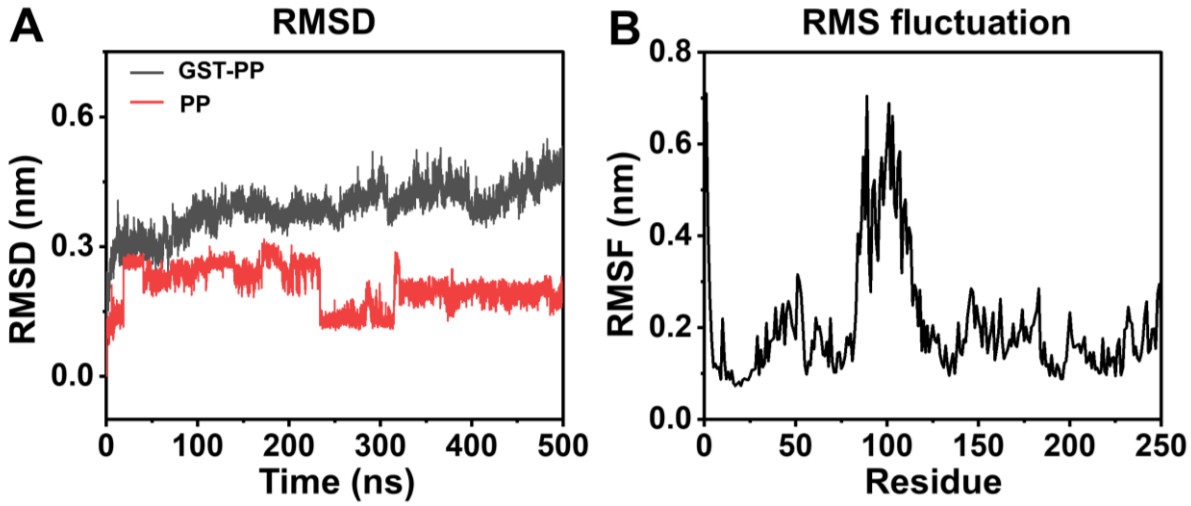

Figure S45. The stability of systems in molecular dynamics simulation of GST-PP. A) Root Mean Square Deviation (RMSD) and B) Root Mean Square Fluctuation (RMSF). The RMSD of a complex is a cumulative measure of all atomic deviations between a given conformation and its target. It serves as a crucial metric for assessing system stability. RMSF, on the other hand, assesses the flexibility or mobility of amino acid residues within a protein. All atoms, including those of the enzyme (e.g., C, O, N, H, S, P atoms, etc.) and the constituent atoms of PP (e.g., C, H atoms), were used to calculate the RMSD. The RMSD values of the protein-substrate complex structures stabilized between 0.3-0.5 nm. In the GST-PP system, the RMSD values of the substrate PP stabilized with fluctuations of ~0.2 nm.

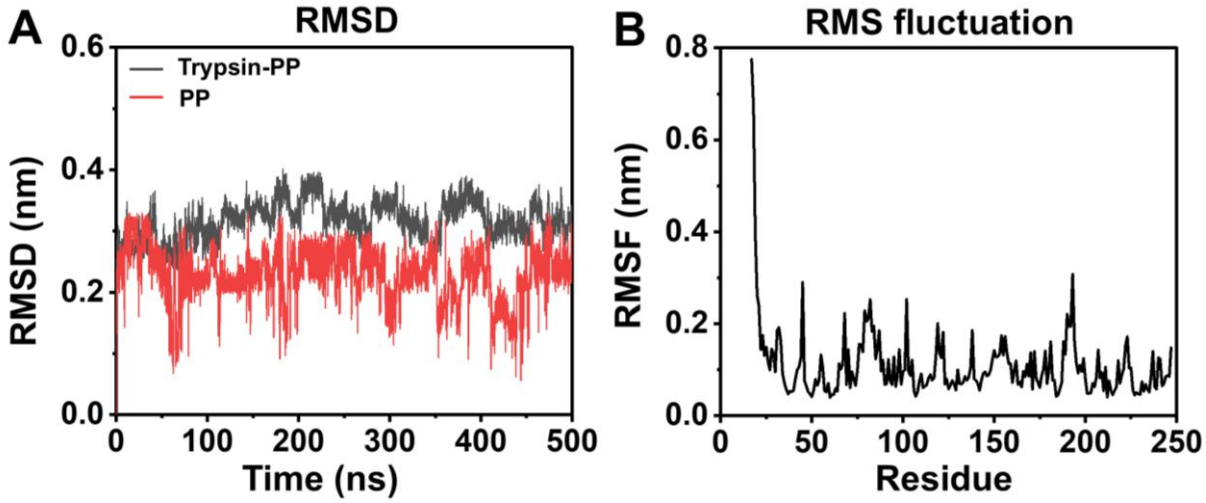

Figure S46. The stability of systems in molecular dynamics simulation of trypsin-PP. A) RMSD and B) RMSF. All atoms, including those of the enzyme (e.g., C, O, N, H, S, P atoms, etc.) and the constituent atoms of PP (e.g., C, H atoms), were used to calculate the RMSD. The substrate PP in trypsin-PP fluctuated between 0.1-0.3 nm.

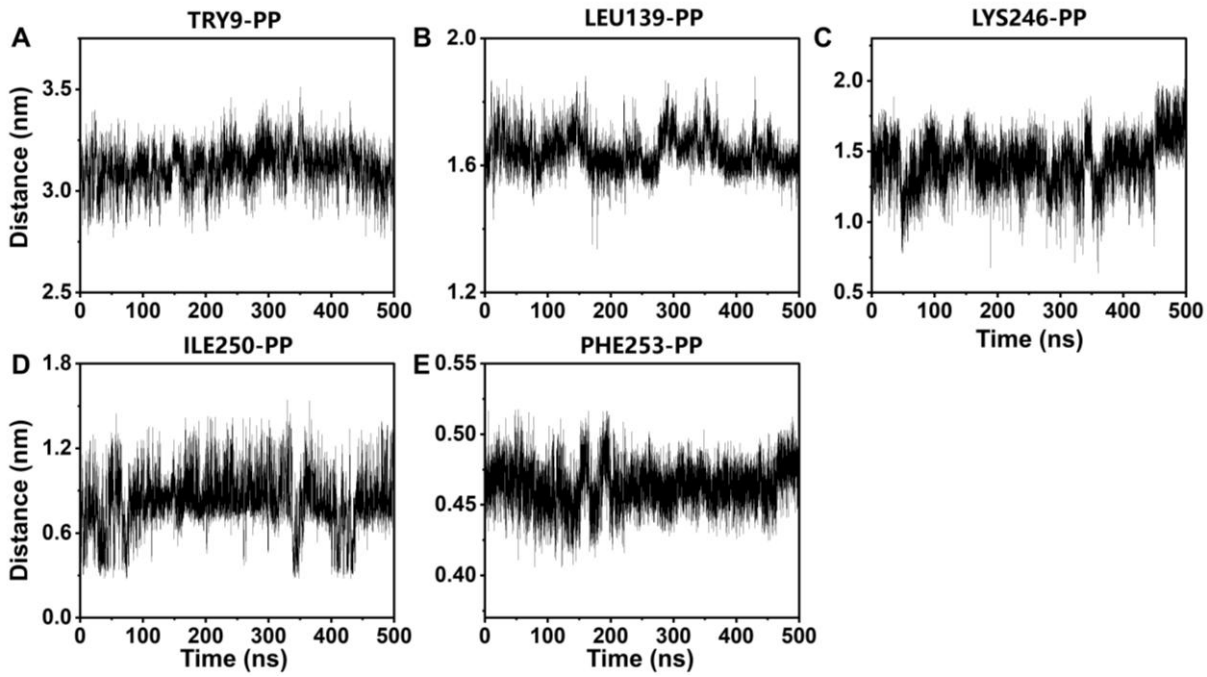

Figure S47. The plots of time dependence evolution of the distance between the key amino acid of GST and PP. It can be seen that the distance between GST and PP exhibited relatively small fluctuations, indicating that they had always been in close proximity. In the final equilibrium state, the distances between PP and key residues stabilized at the following values: approximately 3.1 nm for TRY9, ~1.6 nm for LEU139, ~1.7 nm for LYS246, ~0.9 nm for ILE250, and ~0.5 nm for PHE253.

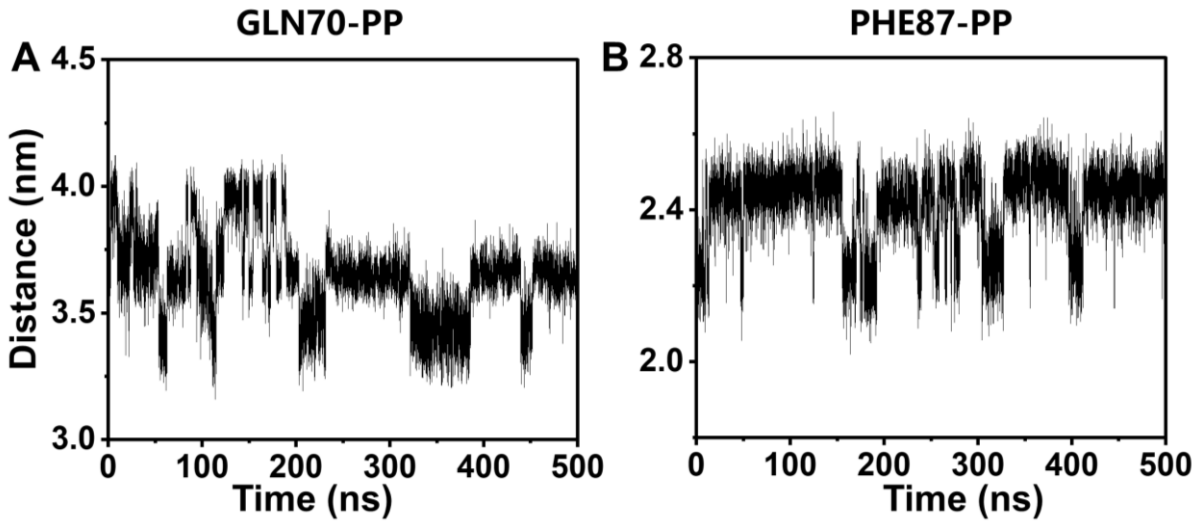

Figure S48. The plots of time dependence evolution of the distance between the key amino acid of trypsin and PP. In the final equilibrium state, the distance between GLN70 and PP stabilized at approximately 3.7 nm, whereas PHE87 and PP maintained a closer proximity of ~2.5 nm (observed between 450–500 ns).

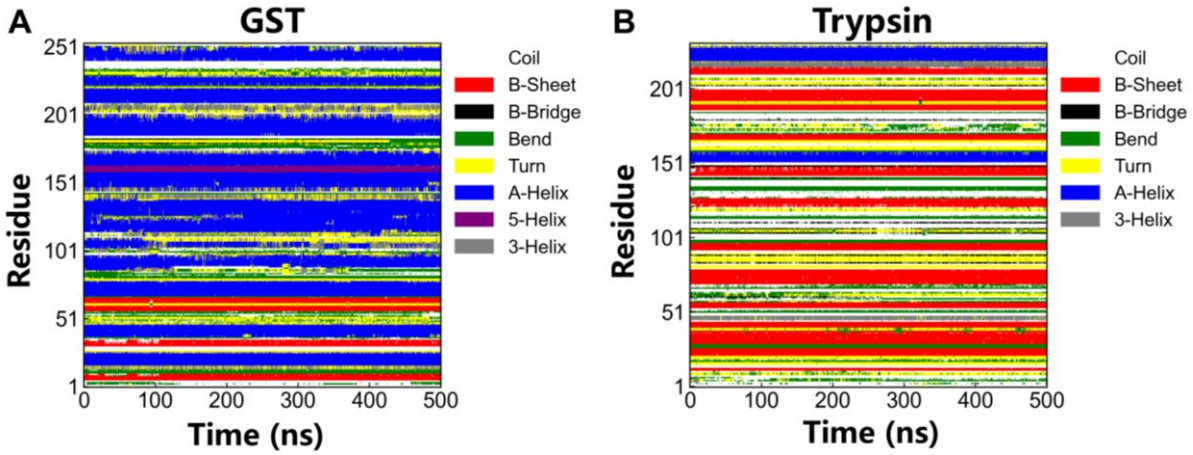

Figure S49. **The secondary structure of A) GST and B) trypsin.**

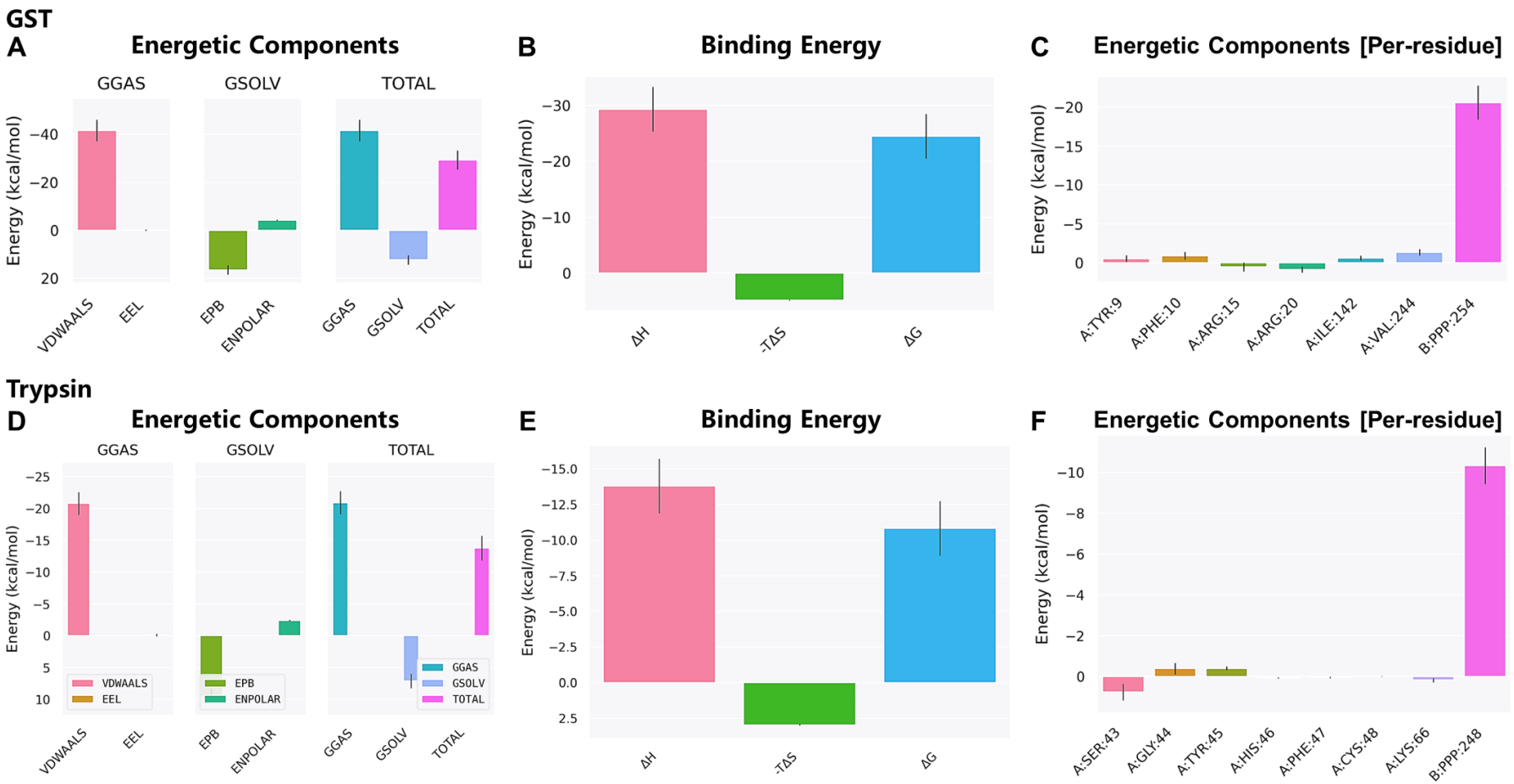

Figure S50. **Intermolecular forces of protein-PP.** A) GST and D) trypsin with PP energetic components and its individual components, Ggas, Gsolv, Gtotal represented van der Waals energy and electrostatic energy, polar solvent energy and SASA energy, the total binding free energy, respectively, B) GST and E) trypsin with PP binding energy, the energy contribution of C) GST and F) trypsin with PP key residues (the ligand around 6 Å residues).

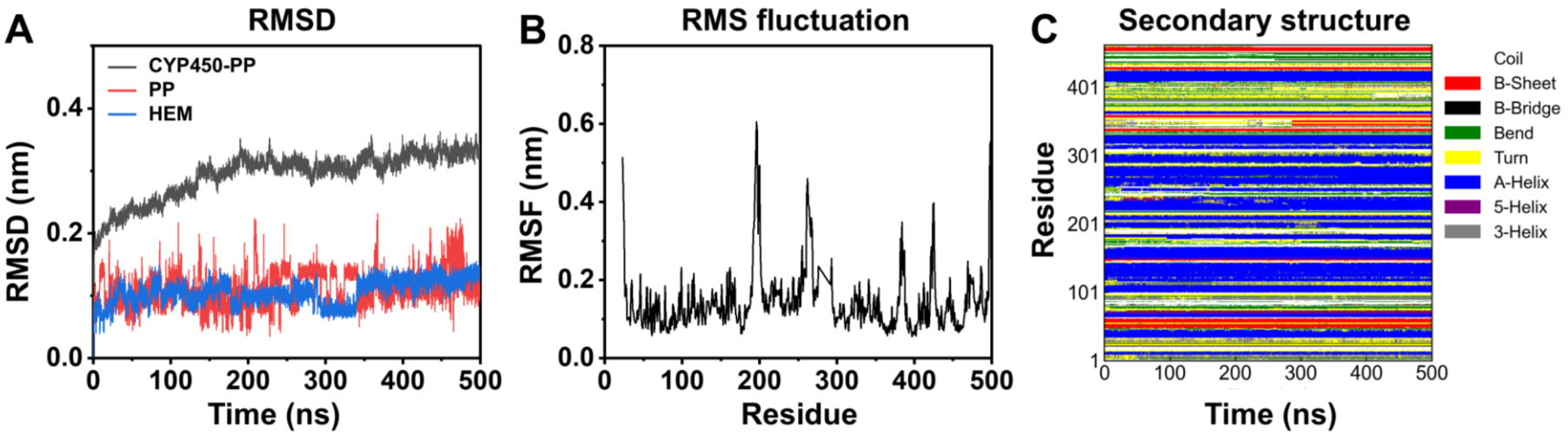

Figure S51. The stability of system in molecular dynamics simulation of CYP450-PP. A) RMSD and B) RMSF. The RMSD of a complex is a cumulative measure of all atomic deviations between a given conformation and its target. RMSF, on the other hand, assesses the flexibility or mobility of amino acid residues within a protein. C) The secondary structure of CYP450.

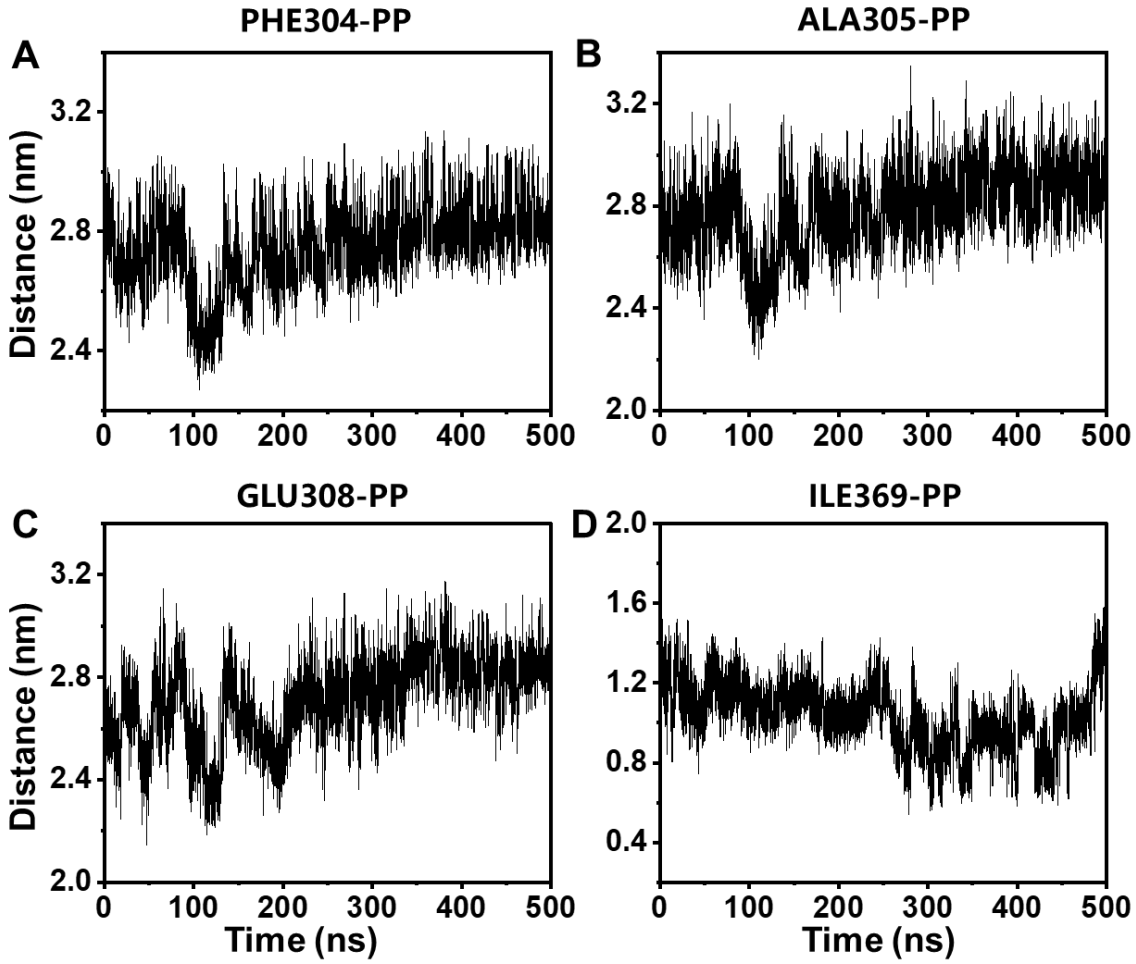

Figure S52. The plots of time dependence evolution of the distance between the key amino acid of CYP450 and PP. It can be seen that the distance between CYP450 and PP remained relatively stable, suggesting that they had consistently been in close proximity. The distances in the final equilibrium state were approximately 2.8 nm for PHE304-PP, 2.9 nm for ALA305-PP and GLU308-PP, and 1.3 nm for ILE369-PP in CYP450-PP system.

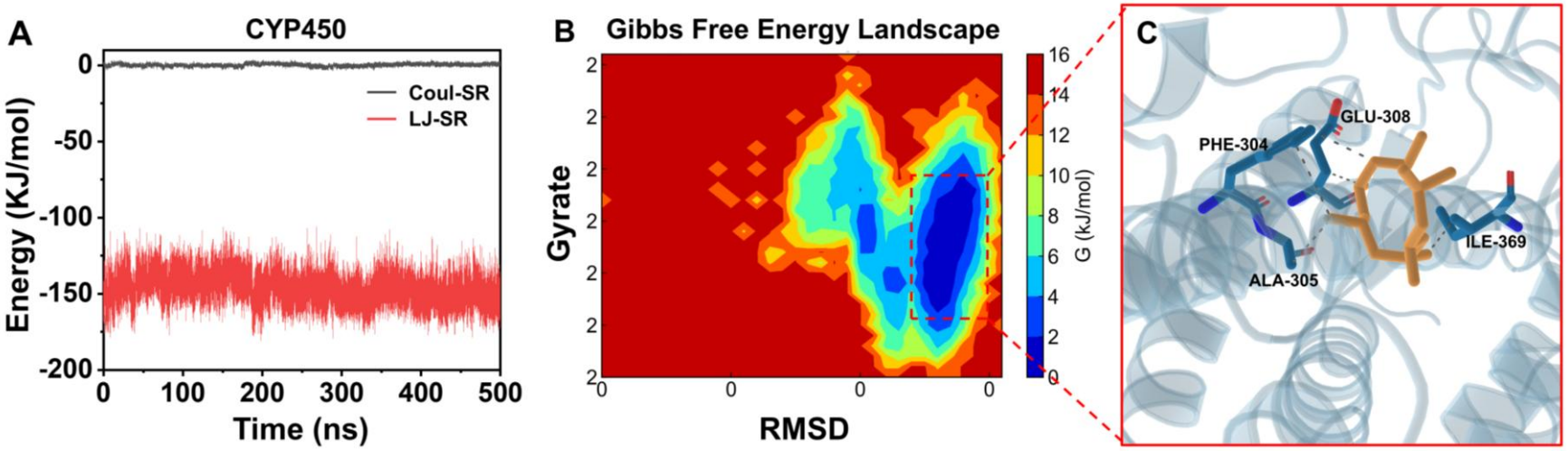

Figure S53. Molecular dynamics simulation of CYP450. A) The potential energy of CYP450 and PP, B) The Gibbs free energy landscape of CYP450-PP, C) The representative structure of the free energy minimum of CYP450-PP complex (hydrophobic interactions shown as gray dashed lines).

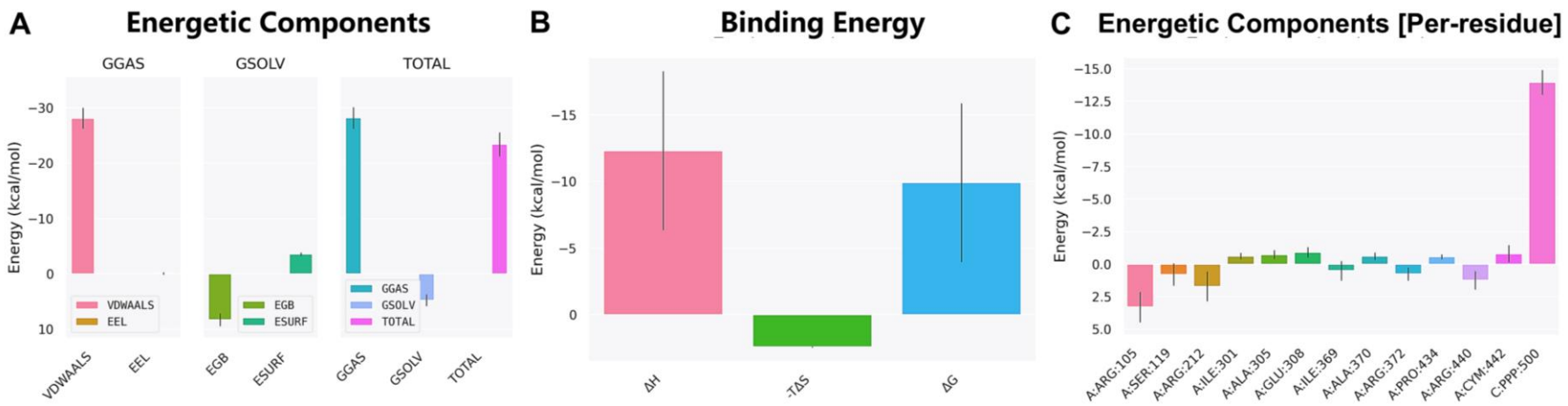

Figure S54. Intermolecular forces of CYP450-PP. A) CYP450 with PP energetic components and its individual components, Ggas, Gsolv, Gtotal represented van der Waals energy and electrostatic energy, polar solvent energy and SASA energy, the total binding free energy, respectively, B) CYP450 with PP binding energy, the energy contribution of C) CYP450 with PP key residues (the ligand around 6 Å residues).

Reference

1. A. Martinsen, G. Skjåk-Bræk, O. Smidsrød, F. Zanetti and S. Paoletti, *Carbohydr. Polym.*, 1991, **15**, 171-193.
2. A. Shrivastava, in *Introduction to Plastics Engineering*, ed. A. Shrivastava, William Andrew Publishing, 2018, DOI: https://doi.org/10.1016/B978-0-323-39500-7.00002-2, pp. 17-48.
3. M. Rogošić, H. J. Mencer and Z. Gomzi, *Eur. Polym. J.*, 1996, **32**, 1337-1344.
4. M. R. Kasaai, *J. Polym. Biopolym. Phys. Chem*, 2018, **6**, 39-44.
5. G. Montaudo, D. Garozzo, M. S. Montaudo, C. Puglisi and F. Samperi, *Macromolecules*, 1995, **28**, 7983-7989.